

CALL FOR PAPERS | *Cardiac Regeneration and Repair: Mechanisms and Therapy*

Antiarrhythmic effect of growth factor-supplemented cardiac progenitor cells in chronic infarcted heart

Monia Savi,*¹ Leonardo Bocchi,*¹ Stefano Rossi,¹ Caterina Frati,² Gallia Graiani,² Costanza Lagrasta,^{2,7} Michele Miragoli,³ Elisa Di Pasquale,^{3,4} Giuliano G. Stirparo,³ Giuseppina Mastrototaro,³ Konrad Urbanek,⁵ Antonella De Angelis,⁵ Emilio Macchi,^{1,7} Donatella Stilli,^{1,7} Federico Quaini,^{6,7} and Ezio Musso^{1,7}

¹Department of Life Sciences, University of Parma, Italy; ²Department of Biomedical, Biotechnological and Translational Sciences, University of Parma, Italy; ³Humanitas Clinical and Research Center, Rozzano (MI), Italy; ⁴Institute of Genetic and Biomedical Research—UOS Milan—National Research Council, Milan, Italy; ⁵Department of Experimental Medicine, Section of Pharmacology, Second University of Naples, Italy; ⁶Department of Clinical and Experimental Medicine, University of Parma, Italy; ⁷Cardiac Stem Cell Interdepartmental Center “CISTAC,” University of Parma, Italy

Submitted 16 January 2015; accepted in final form 10 March 2016

Savi M, Bocchi L, Rossi S, Frati C, Graiani G, Lagrasta C, Miragoli M, Di Pasquale E, Stirparo GG, Mastrototaro G, Urbanek K, De Angelis A, Macchi E, Stilli D, Quaini F, Musso E. Antiarrhythmic effect of growth factor-supplemented cardiac progenitor cells in chronic infarcted heart. *Am J Physiol Heart Circ Physiol* 310: H1622–H1648, 2016. First published March 18, 2016; doi:10.1152/ajpheart.00035.2015.—c-Kit^{pos} cardiac progenitor cells (CPCs) represent a successful approach in healing the infarcted heart and rescuing its mechanical function, but electrophysiological consequences are uncertain. CPC mobilization promoted by hepatocyte growth factor (HGF) and IGF-1 improved electrogenesis in myocardial infarction (MI). We hypothesized that locally delivered CPCs supplemented with HGF + IGF-1 (GFs) can concur in ameliorating electrical stability of the regenerated heart. Adult male Wistar rats (139 rats) with 4-wk-old MI or sham conditions were randomized to receive intramyocardial injection of GFs, CPCs, CPCs + GFs, or vehicle (V). Enhanced green fluorescent protein-tagged CPCs were used for cell tracking. Vulnerability to stress-induced arrhythmia was assessed by telemetry-ECG. Basic cardiac electrophysiological properties were examined by epicardial multiple-lead recording. Hemodynamic function was measured invasively. Hearts were subjected to anatomical, morphometric, immunohistochemical, and molecular biology analyses. Compared with V and at variance with individual CPCs, CPCs + GFs approximately halved arrhythmias in all animals, restoring cardiac anisotropy toward sham values. GFs alone reduced arrhythmias by less than CPCs + GFs, prolonging ventricular refractoriness without affecting conduction velocity. Concomitantly, CPCs + GFs reactivated the expression levels of Connexin-43 and Connexin-40 as well as channel proteins of key depolarizing and repolarizing ion currents differently than sole GFs. Mechanical function and anatomical remodeling were equally improved by all regenerative treatments, thus exhibiting a divergent behavior relative to electrical aspects. Conclusively, we provided evidence of distinctive antiarrhythmic action of locally injected GF-supplemented CPCs, likely attributable to retrieval of Connexin-43, Connexin-40, and Ca_v1.2 expression, favoring intercellular coupling and spread of excitation in mended heart.

cardiac progenitor cells; growth factors and cytokines; myocardial infarction; arrhythmia; cardiac gap junction connexins

NEW & NOTEWORTHY

Repair of infarcted heart by local injection of c-kit^{pos} cardiac progenitors supplemented with hepatocyte growth factor and IGF-1 has distinctive antiarrhythmic effects involving recovery of Connexin-43, Connexin-40, and Ca_v1.2 expression levels differently than progenitors or cytokines alone. This new insight into the impact of regenerative therapies on cardiac electrogenesis has clinical relevance.

HEART FAILURE (HF) very often proceeds as a consequence of myocardial infarction (MI) (59) and continues to be a major health problem (49). Over the past 15 yr, cell therapy has emerged as a new strategy aimed at revitalizing dead myocardium, thus circumventing the unfavorable outcome of degenerative heart diseases, including the vicious circle of MI/HF (67). However, results obtained so far in clinical trials with a large sample size using cells of different origin, mainly skeletal myoblasts (44) and bone marrow cells (78), have been contradictory, with moderate or even no clinical benefits and, in the case of skeletal myoblasts, unwanted complications such as life-threatening arrhythmias. The adverse electrophysiological effects and the limited positive impact on cardiac repair decreased to date the interest in regenerative therapies mediated by skeletal myoblasts (67). As for bone marrow cells, fresh meta-analysis data indicate that the treatment may be advantageous in people with chronic MI and HF, with minimal major intervention-related adverse effects and no increase in the incidence of arrhythmias (23). However, although promising, these results appear to require further research involving larger, appropriately randomized clinical trials (23).

In the last decade, increasing attention has been paid to resident cardiac progenitor cells as a novel target of cell therapy for ischemic cardiomyopathy and failing heart, based on the notion that the adult heart contains progenitors, which are intrinsically programmed to generate myocardium and therefore appear to be best suited for the complex task of reconstituting tissue that is lost with MI (14, 24, 37, 38, 51). By

* M. Savi and L. Bocchi contributed equally to this work.

Address for reprint requests and other correspondence: E. Musso, MD, Dept. of Life Sciences, Parco Area delle Scienze 11/A, I-43124, Parma, Italy (e-mail: ezio.musso@unipr.it).

similar reasoning, stem cells of various origin and more easily harvested than cardiac progenitors, such as mesenchymal and pluripotent stem cells, could be oriented toward cardiac lineages and profitably adopted in clinical settings (45). The initial results of two randomized phase 1 clinical trials (SCIPIO, NCT00474461 and CADUCEUS, NCT00893360), aimed at establishing the feasibility and safety of intracoronary injection of autologous cardiac-derived progenitors in patients with HF after MI, have been published in recent years (7, 42). In the SCIPIO study (7), the infusion of c-kit^{pos} selected cells produced a remarkable improvement in both global and regional left ventricular (LV) function, reduced infarct size, and increased viable tissue. In the CADUCEUS study (42), the administration of cardiosphere-derived cells markedly reduced scar mass and concurrently increased the viable heart mass, regional contractility, and regional systolic wall thickening. In both trials, the improvement in cardiac function persisted at least 1 yr, without any occurrence of major negative consequences attributable to the regenerative treatment. In a third trial (C-CURE, NCT00810238) (2), cardiopoietic stem cells, obtained after exposure of bone marrow-derived mesenchymal stem cells to a cardiogenic cocktail, were delivered to patients with HF of ischemic origin, by endomyocardial injections. Data collected at 6 mo from treatment demonstrated a favorable impact on myocardial remodeling, LV ejection fraction, and global wellness, without any evidence of increased cardiac or systemic toxicity and proarrhythmic risk.

By removing the loss of cardiac tissue as an underlying cause of HF, stem cell-based heart repair is expected to ameliorate both the contractile and the electrical competence of the healed myocardium. Of note, lethal arrhythmias are responsible for up to half of the deaths in HF (30). On the contrary, the arrhythmic risk of implantation, homing, engraftment, and differentiation of regenerating cells within the damaged cardiac tissue has constantly been a reason for major concern in the clinical use (15, 17, 48, 73, 74). Nevertheless, a number of papers documented a direct pro-rhythmic (rather than arrhythmic) action of cell therapy (11, 27, 34, 46, 50, 72, 89, 90, 92, 93).

In preclinical studies, several cohorts of cardiogenic cells were characterized by different groups and considered involved in myocardial renewal (37, 67). Among these populations, although the mechanism is questioned (22, 84), c-kit^{pos} cardiac progenitor cells repeatedly proved capable of rescuing scarred infarcted myocardium and ameliorating cardiac function (4, 5, 80). Additionally, CPCs were reported to express c-Met and IGF-1 receptors and could be activated *in situ* via the corresponding ligands, hepatocyte growth factor (HGF), and IGF-1, promoting repopulation of the damaged heart (21, 33, 39, 64, 82). Activation of CPCs was also obtained either by incubating the cells with HGF and IGF-1 before implantation, or by coinjecting the cells with the two growth factors (GFs) (63, 81). Furthermore, in a rat model of chronic MI, we demonstrated that cardiac repair by local injection of HGF + IGF-1 (GFs) was associated with a decline in proneness to arrhythmias, attributed to better intercellular coupling via increased expression of Connexin-43 (Cx43) and attenuation of negative remodeling (6).

This body of observations formed the basis of the present study aimed at testing the hypothesis that intramyocardial injection of CPCs supplemented with GFs restores electrical function toward normal in the regenerated infarcted heart and also stressing the

potential positive impact of GF adjunct on cardiac performance in cell therapy as well as the differences compared with sole GFs.

MATERIALS AND METHODS

Ethics Statement

The study was conducted in conformity with the American Physiological Society guiding principles in the care and use of vertebrate animals in research and training. The protocol was submitted to, and approved by, the Veterinary Animal Care and Use Committee of the University of Parma and adheres to the National Ethical Guidelines of the Italian Ministry of Health. All surgery was performed under anesthesia, and all animals received humane care.

Animals and Housing

The study population consisted of 157 male Wistar rats (*Rattus norvegicus*) bred in our departmental animal facility, aged 12–14 wk, weighing 350–400 g, and kept under controlled housing conditions (5).

All animals were subjected to either MI or sham operation (SO) and, 4 wk later, treated with GFs, CPCs, CPCs supplemented with GFs, or vehicle (V), representing the following eight groups: MI-GF, MI-CPC, MI-CPC + GF, MI-V, SO-GF, SO-CPC, SO-CPC + GF, and SO-V. Given that in preliminary studies (Fig. 1, A–E), cardiac electromechanical function assessed by vulnerability to arrhythmias and hemodynamic measurements had comparable values in the four SO groups, all so animals of the current study were pooled together and globally defined as SO treated (SO-T). V was normal saline (0.9% wt/vol of NaCl). Eighteen rats died in the perioperative period either before myocardial injection (SO rats, $n = 2$, MI, $n = 7$) or after (MI-V, $n = 4$; MI-GF, $n = 2$; MI-CPC, $n = 1$; MI-CPC + GF, $n = 2$), leaving a total of 139 rats.

Outline of the Experimental Protocols

The experimental design and measurements performed in the various animal groups are summarized in Fig. 2.

Telemetry-ECG, hemodynamics, cardiac anatomy, morphometry, and immunohistochemistry studies. Sixty-four rats were chronically instrumented with a telemetry-ECG system to enable the evaluation of arrhythmia vulnerability in conscious freely moving animals. One week later, a 30-min continuous baseline ECG was recorded to rule out the presence of spontaneous arrhythmias. Four weeks after MI ($n = 45$) or SO ($n = 19$), the animals were investigated for proneness to ventricular arrhythmias by telemetry-ECG recording in baseline condition and stress-induced autonomic stimulation (social stress procedure). All rats were then reoperated on and treated by intramyocardial injections of GFs, CPCs, CPCs + GFs, or V (MI-GF group, $n = 12$; MI-CPC group, $n = 11$; MI-CPC + GF, $n = 12$; MI-V, $n = 10$; SO-T, $n = 19$). In some experiments, enhanced green fluorescent protein-tagged CPCs (GFP^{pos} CPCs) were used for cell tracking. Additionally, selected subgroups of MI animals were chronically instrumented with an osmotic pump for continuous delivery of 5-bromo-2'-deoxycytidine (BrdC), which *in vivo* is metabolically converted to 5-bromo-2'-deoxyuridine (BrdU), to establish the cumulative amount of cell proliferation. Two weeks later, vulnerability to arrhythmias was redetermined by a new series of telemetry-ECG recordings. Afterward, hemodynamic data were invasively collected in all animals listed above and in a further 4 MI-GF, 7 MI-CPC, and 11 MI-CPC + GF. Finally, at death, the heart was perfusion fixed for anatomical, structural, and immunohistochemical studies.

Epicardial multiple lead recording, qRT-PCR, and immunoblot studies. In 51 rats belonging to MI-GF ($n = 11$), MI-CPC ($n = 11$), MI-CPC + GF ($n = 7$), MI-V ($n = 12$), or SO-T ($n = 10$) groups, 2 wk after treatment, electrophysiological investigation was performed by epicardial multiple-lead recording. Sixty-four unipolar electrograms (EGs) were simultaneously collected from as many sites of the

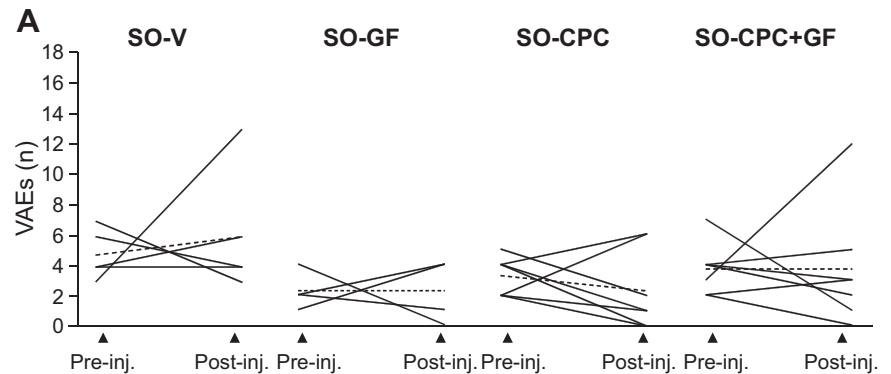
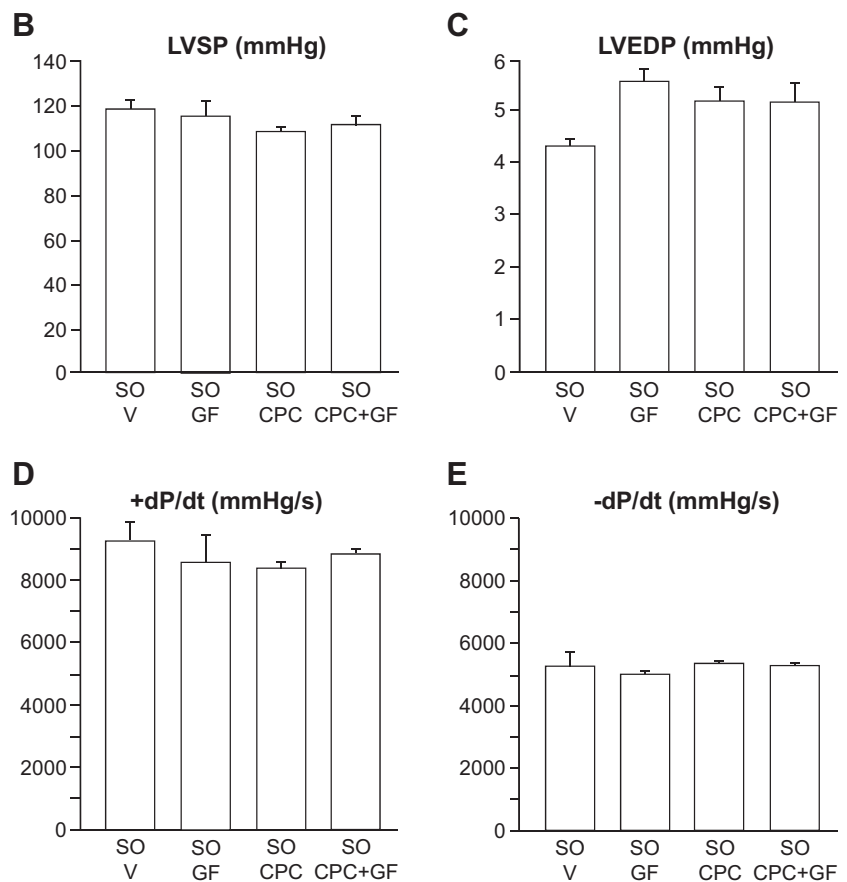


Fig. 1. Different treatments do not impact on proneness to stress-induced ventricular arrhythmias and hemodynamic parameters, in sham-operated (SO) animals. **A**: number of stress-induced ventricular arrhythmic events (VAEs) in SO-vehicle (SO-V) ($n = 6$), SO-growth factor (SO-GF) ($n = 4$), SO-cardiac progenitor cells (SO-CPC) ($n = 7$), and SO-CPC + GF ($n = 7$) groups, before and after injection (Pre-inj. and Post-inj., respectively). In the various plots, continuous lines correspond to individual animals; dashed lines indicate the average behavior within the corresponding group. Data in bar graphs (**B–E**) illustrate the means \pm SE of hemodynamic parameters measured before death in the 4 groups of animals: left ventricular systolic pressure (LVSP; **B**), LV end-diastolic pressure (LVEDP; **C**), maximum rate of ventricular pressure rise ($+dP/dt$; **D**) and reduction ($-dP/dt$; **E**). Functional parameters exhibited comparable values in all experimental groups, independently of the treatment.



infarcted + peri-infarcted epicardial area during sinus rhythm or specific pacing protocols to determine a series of electrophysiological parameters, allowing an in-depth characterization of ventricular electrical function. At death, fresh preparations of the excised heart were immediately frozen for qRT-PCR and immunoblot analyses, which were completed in two supplementary animals assigned to MI-CPC + GF group.

Anesthesia and postinterventional treatment. Animals were anaesthetized with ketamine chloride (40 mg/kg ip; Imalgene; Merial, Milan, Italy) plus medetomidine hydrochloride (0.15 mg/kg ip; Domitor; Pfizer Italia, Latina, Italy) unless otherwise stated. Following the intervention, all animals were given atipamezole hydrochloride (0.15 mg/kg im; Antisedan, Pfizer Italia), flunixin (5 mg/kg im; Finadyne, Schering-Plough, Milan, Italy), and gentamicine sulphate (10 mg/kg im; Aagent; Fatro, Milan, Italy) and kept warm with infrared lamp

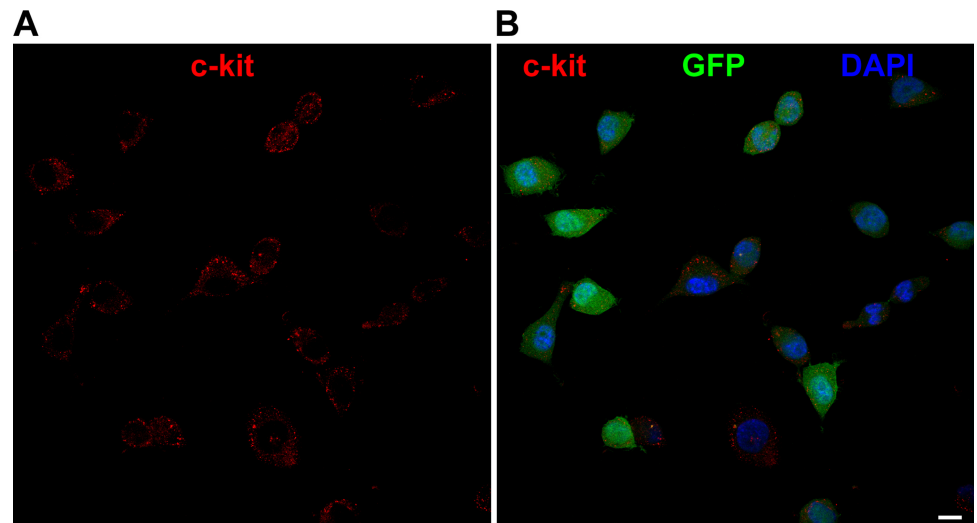
radiation. Eventually, each rat was individually housed, and antibiotic therapy continued for the three subsequent days.

Inclusion criteria for MI and arrhythmias. Because arrhythmogenesis has a multifactorial nature and the occurrence of malignant arrhythmias in subjects with cardiac electrical instability is unpredictable, all anatomically documented MI as well as all ventricular arrhythmic events (VAEs) were included in the study independently of their size and complexity, respectively.

Animal Instrumentation for Telemetry-ECG Recording

Anaesthetized animals (Fig. 2) were chronically instrumented with a miniaturized transmitter for telemetry-ECG recording (model TA11CTA-F40; Data Sciences, St. Paul, MN). The details of the surgical procedure have been published (71).

Fig. 3. CPCs express c-kit, the receptor for stem cell factor. c-Kit labeling (red fluorescence, *A*) is documented in GFP^{pos} (green, *B*) CPCs isolated from GFP-transgenic rats. Scale bar = 10 μ m.



typical preparations, c-kit was expressed in $87.2 \pm 5.4\%$ of isolated CPCs (polyclonal rabbit antibody; Santa Cruz Biotechnology, Dallas, TX; see Table 1). Aliquots were cryopreserved in a medium supplemented with 1% DMSO (Sigma).

Intramyocardial Injection of CPCs

Four weeks after coronary ligation, left lateral thoracotomy was repeated in all animals under anesthesia and mechanical ventilation, as described above. Afterward, selected subgroups of animals were treated with 6×10^5 syngeneic wild-type CPCs or GFP^{pos} CPCs (Fig. 2), suspended in 300 μ l of IMDM supplemented with 1% Pen Strep. CPCs or GFP^{pos} CPCs were delivered in four equally spaced myocardial regions bordering the scar, either alone (MI-CPC hearts) or in combination with HGF (200 ng/ml; PeproTech EC, London, United Kingdom) plus IGF-1 (200 ng/ml; PeproTech EC) (MI-CPC + GF hearts). MI-GF animals were given GFs only. The volume of each injection was 100 μ l. Untreated MI animals (MI-V group) received equal volumes of saline, by the same procedure.

BrdC Administration

In MI animals randomly selected for BrdC administration (Fig. 2), along with surgery for local injection of GFs, CPCs, CPCs + GFs, or V, an osmotic pump (model 2ML4; ALZET; Charles River Laboratories Italia, Calco, Italy) was implanted subcutaneously in the interscapular region to enable a continuous infusion of BrdC 0.6 mol/l (MP Biomedicals Europe, Illkirch, France) at a delivery rate of 2.5 μ l/h. Infusion was maintained until the animals were killed (2 wk). This long infusion time prompted us to use BrdC in place of the most

commonly employed BrdU, owing to the almost sixfold higher solubility of BrdC (which in vivo is metabolically converted to BrdU, as mentioned above).

Hemodynamic Study

Animals (Fig. 2) were anesthetized with droperidol + fentanyl citrate 1.5 mg/kg im (Leptofen; PHARMACIA & UPJOHN, Milan, Italy), which, in our experience, exerts negligible effects on hemodynamic parameters.

The right carotid artery was cannulated with a microtip pressure transducer catheter (Millar SPC-320; Millar Instruments, Houston, TX) connected to a recording system (Power Laboratory ML 845/4 channels; 2Biological Instruments, Besozzo, Italy), and both systolic and diastolic blood pressures were determined. The catheter was then advanced into the LV to measure: 1) LV systolic pressure (LVSP); 2) LV end-diastolic pressure (LVEDP); 3) maximum rate of ventricular pressure rise (+dP/dt) and reduction (−dP/dt), taken as indexes of ventricular mechanical efficiency; 4) isovolumic contraction time (IVCT, duration of isovolumic contraction, computed from LVEDP to the time of aortic valve opening); 5) LV relaxation time (IVRT, duration of isovolumic relaxation, computed from −dP/dt to 5 mmHg above LVEDP), and 6) ejection time (ET, approximated as the time interval between aortic valve opening and time of −dP/dt) (software package AcqKnowledge 3.9; Biopac Systems, Goleta, CA). Eventually, we computed the myocardial performance index (MPI) as the ratio of total time spent in isovolumic activity (IVCT + IVRT) to ET: (IVCT + IVRT)/ET (66). MPI is considered to reflect global cardiac function and possess prognostic value after MI (47).

Table 1. List of antibodies employed for immunohistochemistry

Epitope	Origin	Dilution, Incubation	Company
GFP	Polyclonal goat	1:100, 60' 37°C	Abcam (Cambridge, UK)
	Polyclonal chicken	1:100, 60' 37°C	Abcam
BrdU	Monoclonal mouse	1:20, 90' 37°C	Dako (Glostrup, Denmark)
α -SA	Monoclonal mouse	1:100, 37°C o.n.	Neomarkers (Milan, Italy)
Cx43	Polyclonal rabbit	1:100, 60' 37°C	Sigma (Milan, Italy)
Cx40	Polyclonal rabbit	1:250, 90' 37°C	Abcam
α -SMA	Monoclonal mouse	1:50, 37°C o.n.	Dako
Ki-67	Polyclonal rabbit	1:200, 4°C o.n.	Abcam
vWF	Polyclonal rabbit	1:100, 37°C o.n.	Dako
c-kit	Polyclonal rabbit	1:100, 60' 37°C	Santa Cruz Biotechnology (Dallas, TX)
CD31/PECAM-1	Polyclonal goat	1:150, 60' 37°C	Santa Cruz Biotechnology

GFP, green fluorescence protein; BrdU, bromo deoxyuridine; α -SA, α -sarcomeric actin; Cx43, Connexin-43; Cx40, Connexin-40; α -SMA, α -smooth muscle actin; vWF, von Willebrand factor; CD31/PECAM-1, CD31/platelet endothelial cell adhesion molecule-1; o.n., overnight.

Epicardial Multiple-Lead Recording

Animals under anesthesia and artificially ventilated (Fig. 2) were subjected to left thoracotomy. Body temperature was held constant at 37°C by infrared lamp radiation. Sixty-four unipolar EGs were simultaneously recorded from the epicardial surface via an 8 × 8 row and column electrode array with 1-mm interelectrode distance. The array was positioned over the infarcted region and the surrounding areas, just below the site of coronary ligation. The details of the surgical approach, the construction of the multiple electrode grid, and the recording system have already been described (40). EG recordings were performed during normal sinus rhythm or pacing by specific protocols at 4–18 selected electrodes of the array (Fig. 4A), using near-threshold, ≤1-ms cathodal current pulses, at a frequency as specified when appropriate. During pacing, EGs were obtained from all the electrodes except at the paced site (Fig. 4B). As indicated earlier (6), in some cases, the proper positioning of the array on the ventricular epicardium was prevented by an unfavorable spatial relationship between heart and lungs in the open chest preparation. Because of this and the presence of scattered fibrotic areas in the infarcted region, only a fraction of the 64 sites explored by epicardial electrodes was excitable and/or enabled the recording of reliable EG signals. The measurements were carried out in accordance with standard procedures (35, 40, 52) and included conduction velocity (CV), excitability, refractoriness, dispersion of refractoriness, and quantification of spatial inhomogeneity in conduction.

Conduction velocity. Activation time at each electrode site was estimated using the instant of the minimum time derivative of unipolar EG during QRS and was referenced to stimulus onset of paced beats at a frequency slightly higher than spontaneous sinus rhythm (basic cycle length, BCL ≈ 300 ms). From the activation times, an activation

sequence (isochrone map) was determined where CV was computed longitudinally (CV-l) and transversally (CV-t) to epicardial fiber orientation (Fig. 4C), as previously detailed (6, 79).

Excitability. Four to eight selected electrodes of the array (Fig. 4A) were initially paced at BCL with current pulses of decreasing strength (starting from supraliminal values) at a constant duration of 5 ms until activation failed, thus identifying the threshold current. The procedure was then repeated with current pulses of progressively shorter duration, down to 0.01 ms. The threshold currents as a function of pulse duration defined the strength-duration (S-D) curve from which the related parameters Rheobase (Rh) and Chronaxie (Chr) were obtained, univocally identifying the S-D curve and thus characterizing tissue excitability (6, 10) (Fig. 4D).

Refractoriness. At each of the 4–18 selected electrodes of the array (Fig. 4A), eight BCL stimuli (S1), 1-ms duration and twice diastolic threshold current strength, were delivered. The S1 pacing sequence was followed by an extra stimulus (S2) whose delay from previous S1 was first progressively decremented by 10-ms steps until capture was lost and then progressively incremented by 2-ms steps until capture was resumed. The longest S1-S2 coupling interval that did not originate ventricular capture identified the effective refractory period (ERP) at a given electrode site, enabling the characterization of spatial differences in tissue refractoriness.

Dispersion of refractoriness. The degree of dispersion was evaluated by computing the ERP dispersion value taken as a basic indicator of propensity to reentrant arrhythmias (54) and, in an individual animal, was expressed by the standard deviation of the mean ERP at all test sites (52).

Quantification of spatial inhomogeneity in conduction. Given the recognized significance of spatial inhomogeneities in propagation for

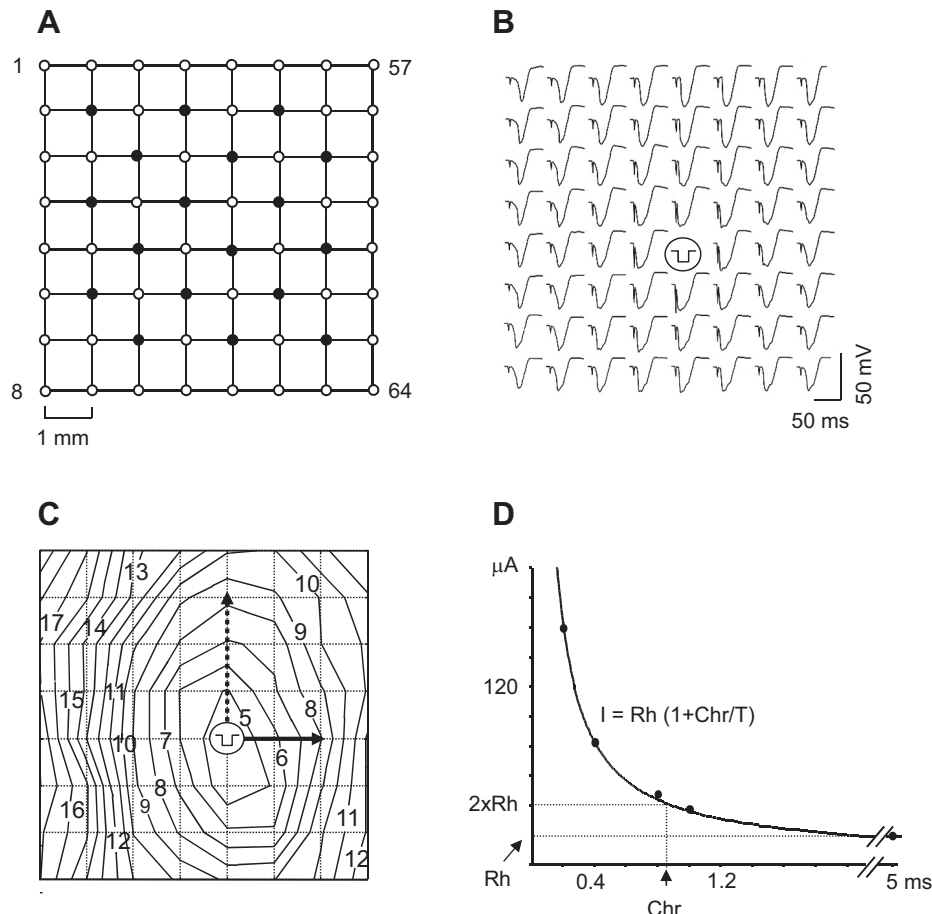


Fig. 4. Epicardial multiple-lead recording: electrode array and procedures. A: schematic representation of the 8 × 8 electrode array showing the positions (●) of the 18 selected electrodes used for specific pacing protocols. B: unipolar electrograms collected by means of the electrode array during ventricular pacing at the electrode indicated by the pulse symbol. C: example of paced activation isochrone map used for computing conduction velocity longitudinally (dashed arrow) and transversally (solid arrow) to epicardial fiber orientation. Numbers on each isochrone line indicate the activation time in ms. D: strength-duration curve obtained in a control rat by plotting pulse threshold current I as a function of pulse duration T . Rh is the Rheobase, i.e., the lowest current strength with infinite pulse duration, which succeeds in eliciting a propagated response in excitable tissues. Chr is the Chronaxie, i.e., the pulse duration having a threshold current strength twice that of Rh.

the initiation of reentrant arrhythmias, maps of spatial distribution of inhomogeneities in conduction (phase maps) were obtained from isochrone maps, in accordance with Lammers et al. (35). Briefly, the local phase differences in activation times were calculated for each quadruplet of neighboring recording points. The total population of phase differences were then plotted as a histogram and described by percentile scores. The total range in maximal differences in activation times (P_{5-95}) was used to express the absolute inhomogeneity in conduction. The variant coefficient (P_{5-95}/P_{50}) was used as an inhomogeneity index to express the local inhomogeneity independent of conduction velocity. In each animal, four phase maps were obtained by impulse delivered at as many stimulating points, at BCL driving frequency.

Cardiac Anatomy

The heart of anesthetized animals (Fig. 2) was arrested in diastole by injection of 5 ml of cadmium chloride (100 mmol/l iv) and briefly perfused at physiological mean arterial blood pressure with heparinized PBS, followed by 10-min perfusion with 10% of formalin solution. The heart was excised and fixed for 24 h in 10% formalin, and the right ventricle and the LV, including the septum, were separately weighed. The volume of the LV myocardium was computed by dividing the ventricular weight by the specific gravity of the tissue (1.06 g/ml). The major cavitory axis of the LV was measured from the aortic valve to the apex under a stereomicroscope with a ruler calibrated exactly to 0.1 μ m (2Biological Instruments). Subsequently, the LV was sliced in three transverse sections corresponding respectively to the base, equatorial portion, and apex. On the equatorial section, LV wall thickness and LV chamber diameter were measured using software for image analysis (Image Pro-plus, version 7.0; Media Cybernetics, Rockville, MD). LV chamber volume was calculated according to the Dodge equation, which equalizes the ventricular cavity to an ellipsoid (19). Finally, the basal, equatorial, and apical sections were embedded in paraffin, and 5- μ m-thick slices were cut for morphometric and immunohistochemical studies.

Morphometric Analysis

In rat hearts from the different groups (Fig. 2), infarct size was morphometrically evaluated according to a methodology repeatedly employed in our laboratory (6). Briefly, hematoxylin and eosin-stained sections were analyzed, and the quotient between the number of myocytes present in the infarcted portion of LV and the number of LV myocytes in the corresponding portion of SO hearts represented the quantitative measurement of infarct size. The newly formed myocardium in treated hearts was not included in this analysis so as to ascertain the consequences of coronary ligation on infarct size, independently of tissue reconstitution.

In the same animals, 5- μ m-thick slices from the LV equatorial section stained with Masson's trichrome were analyzed via optical microscopy (magnification $\times 250$) to evaluate in the remote and peri-infarcted spared myocardium, namely 1) the volume fraction of myocytes and 2) the volume fraction of diffuse and replacement fibrosis. As previously reported (77), on each slice, this analysis was performed in 60 adjacent fields from subendocardium to subepicardium, with the aid of a grid defining a tissue area of 0.160 mm² and containing 42 sampling points. The number of points overlying cardiomyocytes and fibrotic tissue was counted and expressed as a percentage of the total number of points explored.

Finally, the cross-sectional area of cardiomyocytes in the spared myocardium was morphometrically determined by measuring the cell diameter at the level of the nucleus, in transversally oriented cells. On each heart, 120–250 individual measurements were performed.

Immunohistochemistry

Six randomly selected MI-V and MI-GF rat hearts and as many MI-CPC and MI-CPC + GF, among those injected with GFP^{pos}

CPCs, were subjected to immunohistochemical studies (Fig. 2). Five-micrometer-thick LV sections were analyzed by confocal microscopy (Zeiss 510 meta confocal microscope) to determine 1) the number of engrafted GFP^{pos} CPCs and their differentiation into cardiac lineages, 2) the fraction of BrdU-labeled nuclei in the infarcted + peri-infarcted LV myocardium, and 3) the expression and spatial distribution of Cx43 and Cx40. GFP, α -sarcomeric actin (α -SA), α -smooth muscle actin (α -SMA), von Willebrand factor, CD31/platelet endothelial cell adhesion molecule-1 (CD31/PECAM-1), Ki-67, connexins, and BrdU were detected via specific antibodies and immunofluorescence. For this purpose, LV sections were incubated with the primary antibody (Table 1) followed by exposure to FITC-, tetramethylrhodamine isothiocyanate-, or Cyanine5-conjugated donkey secondary antibodies (Jackson Laboratory, Bar Harbor, ME) to simultaneously detect different epitopes. To ascertain the expression of GFP and to avoid cross reactivity when multiple epitopes were to be investigated, two different GFP primary antibodies were employed, as appropriate (Table 1). Nuclei were stained by DAPI (Sigma). A cover slip was mounted with Vectashield (Vector Laboratories, Burlingame, CA) on each slide for fluorescence microscopy.

The quantitative measurement of Cx43 and Cx40 immunofluorescent signals was performed in the zone bordering the infarct. After immunostaining, microscopic images were recorded with identical acquisition parameters in areas of comparable size and orientation of cardiomyocytes. As fibroblasts from the infarcted areas are known to express connexins (12), to achieve reliable information on connexin density in the myocyte compartment, the zones occupied by interstitial fibroblasts and coronary vasculature were excluded from the analysis by morphology. Sampling involved a minimum of 0.75 mm² to a maximum of 1.2 mm² of myocardium for each connexin immunolabeling, in each experimental group. The area and the intensity of fluorescence of each spot were measured with the Image Pro-plus software. On the basis of the notion that intensity and size of individual areas occupied by fluorescence signals distribute over a rather wide value interval, we applied a corrected quantification approach by computing the data of fluorescence intensity, spot dimension, and number of spots relative to the myocardial tissue unit area.

CPC engraftment and differentiation were determined by analyzing a minimum of 1.12 mm² up to a maximum of 3.89 mm² of myocardium on each GFP^{pos} CPC-injected rat heart. An overall area of 63.39 mm² and 61.93 mm² of myocardium was analyzed in MI-CPC and MI-CPC + GF rats, respectively. The amount of newly formed myocardium was computed by calculating the number of small GFP^{pos}/ α -SA^{pos} myocytes following a previously described methodology (6).

Finally, the density of resistance arterioles and capillary (n/mm²) in surviving myocardium was measured by counting respectively vascular and microvascular profiles labeled by anti- α -SMA and CD31/PECAM-1 antibodies.

mRNA Expression of Connexins, Ion Channels, and Adrenergic Receptors by qRT-PCR.

We assessed the mRNA expression level of major connexins in the conductive and working myocardium (Cx43, Cx40, and Cx45) as well as the channel proteins of 1) depolarizing ion currents: I_{Na} ($Na_v1.5$), $I_{Ca,L}$ ($Ca_v1.2$), and $I_{Ca,T}$ ($Ca_v3.1$) and 2) repolarizing ion currents: I_{to} ($K_v4.2$, $K_v4.3$, $K_v1.4$), I_{Kr} ($K_v11.1$), I_{Ks} ($K_v7.1$), and I_{K1} ($K_v2.1$, $K_v2.2$). Transcripts of adrenergic β 1- and β 2-receptors were also determined. The analysis was performed on the infarcted + peri-infarcted myocardium of 4 SO-T, 2 MI-GF, 2 MI-V, 4 MI-CPC, and 4 MI-CPC + GF animals, in technical triplicate for each heart (Fig. 2). Briefly, after homogenization of the tissues, total RNA was extracted using TRIzol reagent (Invitrogen, Life Technologies, Monza, Italy) according to the manufacturer's recommendations. The quantity and the quality of total RNA were assessed by absorbance 260 nm and 280 nm and by gel electrophoresis. One microgram of total RNA was

reverse transcribed using high-capacity cDNA reverse transcription kit (Applied Biosystems Italia, Monza, Italy). Reverse transcription was performed at 25°C for 10 min, 37°C for 120 min, and stopped by incubating at 85°C for 5 s. Gene expression was assessed by real-time qPCR (7900HT, Applied Biosystems) using GoTaq qPCR master mix syber green (Promega Italia, Milan, Italy) and specific primers (Table 2). Primers and probes were obtained from Applied Biosystems and Sigma. Expression values were presented using the $\Delta\Delta C_T$ and normalized to the housekeeping gene (cyclophilin, kindly provided by Dr. Quintavalle, Humanitas Research Center, Rozzano, Italy). Results are reported as means \pm SE of $-\Delta\Delta C_T$ values.

Electrophoretic and immunoblot analysis.

The infarcted + peri-infarcted portions of the LVs obtained from 2 SO-T, 2 MI-V, 2 MI-GF, 3 MI-CPC, and 4 MI-CPC + GF animals (Fig. 2) were immediately frozen at -80°C . For immunoblot assay of Cx43 and Cx40, the fresh ventricular tissue was mechanically fragmented in liquid nitrogen and lysed with 300 μl of lysis buffer containing the following (all from Sigma): protease (1:100) and phosphatase (1:100) inhibitors, NaCl (150 mmol), Tris-HCl (50 mmol), EDTA (5 mmol), Nonidet P-40 (1%), sodium fluoride solution (10 mmol), sodium diphosphate dibasic (10 mmol), SDS (0.1%), and sodium deoxycholate (0.5%). For each animal, equivalents of 50 μg of protein were separated by 10.5% SDS-PAGE. Coomassie blue dye was used for staining proteins in SDS-PAGE gels and to check the quality of each sample. After electrophoresis, the proteins were transferred onto nitrocellulose membranes to perform the antibody detection. Membranes were blocked with 5% milk in Tris-buffered saline with Tween-20 (Sigma) and incubated overnight at 4°C with the primary polyclonal rabbit anti-Cx43 antibody (1:8,000; Abcam, Cambridge, MA), or the primary polyclonal rabbit anti-Cx40 antibody (1:2,000, Abcam). The second incubation was performed for 1 h at room temperature with peroxidase-conjugated affinity-purified goat anti-rabbit secondary antibody (Bio-Rad Laboratories, Hercules, CA). Peroxidase activity was developed using the enhanced chemiluminescence Western blotting system (Amersham Rahn, Zürich, Switzerland), according to the manufacturer's instructions. To determine the expression levels of Cx43 and Cx40, blots were scanned, and the intensity of the band was quantified by means of the ImageJ Program (NIH, Bethesda, MD). All measurements were performed in technical triplicate. Actin was used as the loading control (primary polyclonal rabbit anti-actin antibody, 1:5,000; Sigma). More than one gel was used for determining the average value of each protein because our set-up for Western blot assay allows running only eight samples simultaneously. Thus to obtain measurements in triplicate for every connexin protein in each sample (2 SO-T, 2 MI-V, 2 MI-GF, 3 MI-CPC, and 4 MI-CPC + GF), we ran the samples together with the

internal control (actin) five times. For each run, the 2 SO-T samples were always present.

Statistical Analysis

The SPSS statistical package was used (version 18; SPSS, Chicago, IL). Normal distribution of variables was checked by means of the Kolmogorov-Smirnov test. Statistics of variables included means \pm SE, paired Student's *t*-test, χ^2 test, one-way ANOVA (post hoc analyses: Bonferroni test or Games-Howell test, when appropriate), and linear correlation analysis. For immunoblot data, nonparametric Kruskal-Wallis test followed by individual Mann-Whitney *U*-test was used. Statistical significance was set at $P < 0.05$.

RESULTS

Telemetry-ECG Data: Proneness to Arrhythmias in Conscious, Freely Moving MI Rats Was Lowered by GFs and Even More GF-Implemented CPCs

Arrhythmia vulnerability was evaluated as the number of VAEs during 15-min baseline and stress-induced sympathetic stimulation periods. In the various trials, VAEs were represented by isolated premature beats, some couplets, and, in several instances, more complex patterns, mainly found in rats with MI (Fig. 5A). Before injection of GFs, CPCs, CPCs + GFs, or V, a few VAEs occurred in MI rats during baseline (average number: 4.5 ± 1.6), whereas stress VAEs were documented in both SO and MI animals, but at a higher level in the latter group (3.2 ± 0.3 vs. 9.9 ± 0.2 ; $P < 0.01$). After injection, stress VAEs did not vary significantly in SO-T and MI-V and MI-CPC rats compared with preinjection values (Fig. 5, B, C, and E). In contrast, the coinjection of CPCs and GFs significantly reduced stress VAEs by about half ($P < 0.02$ vs. preinjection values, Fig. 5F) in all animals. GFs alone too succeeded in diminishing stress VAEs ($P < 0.05$ vs. preinjection values; Fig. 5D) yet in a lower percentage of animals (67 vs. 100%, $P < 0.05$, χ^2 test, Fig. 5D). By these data, GF adjunct appeared to exert a pivotal role in restoring ventricular electrical stability in CPC-mediated repair of chronic MI, whereas GFs alone had smaller beneficial effects.

Furthermore, telemetry-ECGs were subjected to time-domain analysis of heart rate variability (75) to assess whether the reduced arrhythmic risk in MI-CPC + GF and MI-GF animals was related to changes in cardiac autonomic input, which were

Table 2. Primers for quantitative RT-PCR analysis

Gene	Protein	Forward	Reverse
GJA1	Cx43	TTGTTTCTGTACACAGTAAC	GATGAGGAAGGAAGAGAAGC
GJA5A	Cx40	CTGGCCAAGTCACGGCAGGG	TTGTCACTGTGGTAGCCCTGAGG
GJA7	Cx45	GGGCAAAACCAATTCACACAC	CAAGATTAATCCAGACGGAG
SCN5A	Na _v 1.5	TCCTGAGAGCTCTGAAAACCA	GATTAGGGCTCCCACGATG
CACNA1c	Ca _v 1.2	AAGGTGGTACACGAAGCTCAA	CGTGGGCTCCCATAGTTG
CACNA1 G	Ca _v 3.1	ACACACCACTGCCACATT	GGGAGATGGTGTCAAAACAGC
KCND2	K _v 4.2	CAGCTTCGAGACACAACACC	TGTTTCATCCACAACCTCATGG
KCND3	K _v 4.3	GTGGATGATCCCTGTTGTC	TGCTCATCAATAAATCGTGGT
KCNA4	K _v 1.4	ACAGCCACATGCCTTATGGT	GCAAGTCTCTCCCTCTCTCG
KCNH2	K _v 11.1	GATCGCCTTCTACCGGAAA	CCCATCCTATTCTTCACG
KCNQ1	K _v 7.1	AGCAGTATGCCGCTCTGG	CTCTGTCCCAAAGAACACCAC
KCNJ2	K _{ir} 2.1	TGGGAGAGAAAGGACAGAGG	AAAACAGCAATCGGGCACT
KCNJ12	K _{ir} 2.2	GGCATCATCTTCTGGGTCAAT	AGTCTGTGCTCGCTTCTTGG
ARDB1	BETA-1	AGAGCAGAAGCGCTCAAG	AGCCAGCAGACCGTGAAC
ARDB2	BETA-2	TGCTATCACATCGCCCTTC	ACCACTCGGGCCTTATTCTT

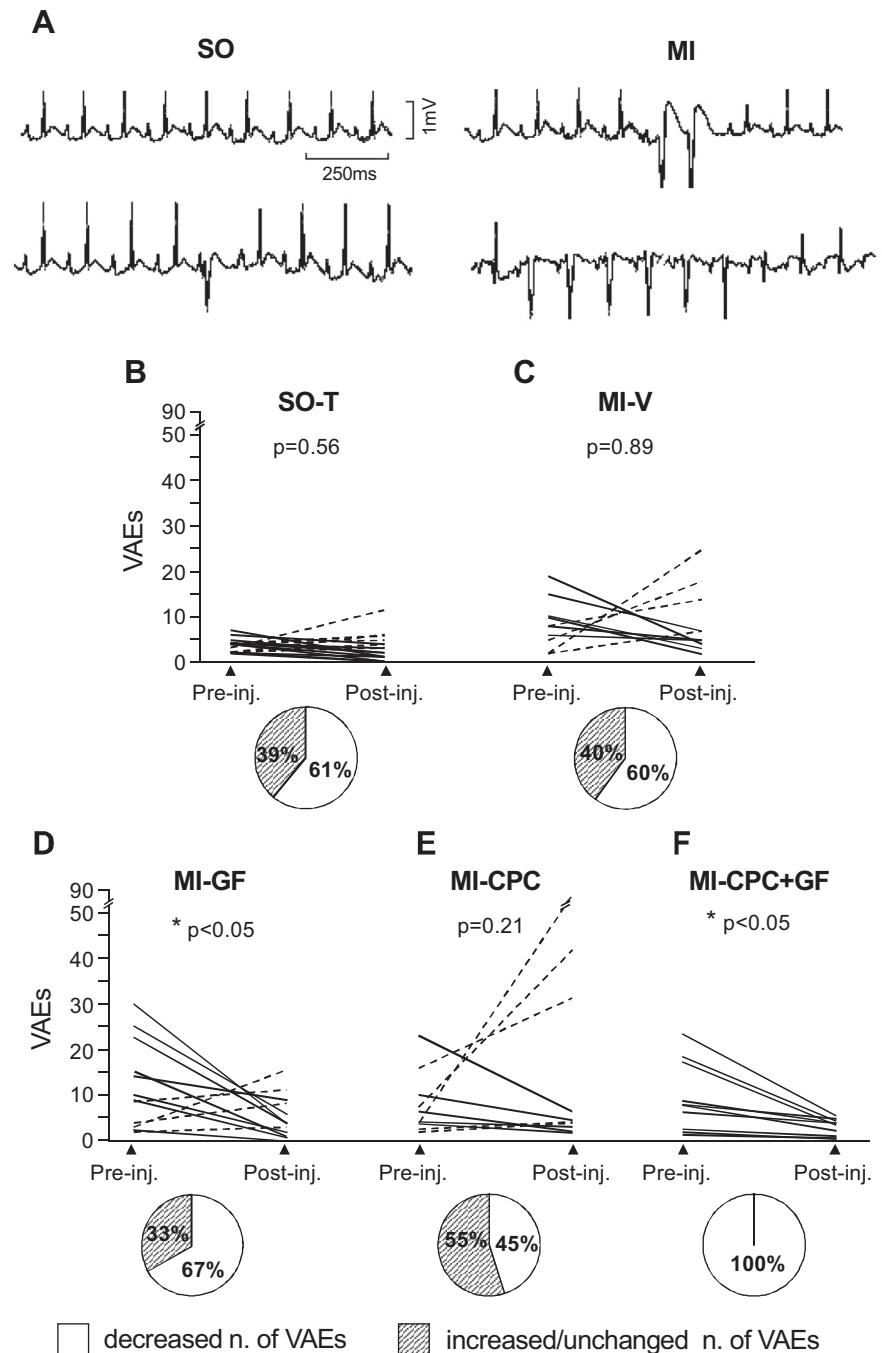


Fig. 5. Local injection of GFs and even more CPCs + GFs reduced the proneness to stress-induced arrhythmias in chronic MI. **A**: telemetry-ECG recorded during social stress exposure showing the different types and severity of VAEs, in representative SO (left) and MI animals (right). **B–F**: effect of different treatments on the number of stress-induced VAEs in SO-T (**B**; $n = 19$), MI-V (**C**; $n = 10$), MI-GF (**D**; $n = 12$), MI-CPC (**E**; $n = 11$) and MI-CPC + GF (**F**; $n = 12$) groups. In each plot, lines correspond to individual animals exhibiting a decline (continuous line) or rise/no change (dashed line) in number of VAEs. The percentage of rats with a decreased number of VAEs within each group is shown by the pie chart, at the bottom of the corresponding plot. * $P < 0.05$ vs. preinjection values, in MI-GF and MI-CPC + GF groups (paired t -test).

reported to be involved in arrhythmias following regenerative therapies (56, 92). During baseline, the indexes of heart rate variability SDRR and r-MSSD were similar in the different groups (Table 3), before and after injection. The rise in sympathetic tone brought about by the social challenge (70) reduced SDRR and r-MSSD by nearly 45 and 30%, respectively ($P < 0.05$) in the various animals, with no difference before and after treatment. Likewise, R-R interval during both baseline and stress conditions did not differ in the five rat groups (Table 3).

Finally, in accordance with previous studies (8, 9, 28), LV β -receptor transcript levels either were not affected by MI (BETA-2) or were reduced (BETA-1). In the latter case, the

decline was evenly restored by GF, CPC, and CPC + GF treatments (Fig. 6). Thus direct and indirect markers of the autonomic input to the heart had comparable values in the three cured MI groups.

Epicardial Multiple-Lead Recordings: Negative Remodeling of Basic Cardiac Electrophysiological Properties After MI Was Restored in a Different Way by Regenerative Treatments

The electrophysiological mechanisms underlying the antiarrhythmic effects of CPCs + GFs compared with sole CPCs or GFs were explored at tissue level by epicardial measurements

Table 3. R-R interval and R-R variability indexes

Groups	R-R Baseline, ms	R-R Stress, ms	SDRR Baseline, ms	SDRR Stress, ms	r-MSSD Baseline, ms	r-MSSD Stress, ms
<i>Preinjection</i>						
SO (<i>n</i> = 19)	175 ± 2	124 ± 1*	11.7 ± 0.5	7.0 ± 0.6*	4.0 ± 0.3	3.0 ± 0.1*
MI (<i>n</i> = 45)	173 ± 3	122 ± 1*	11.5 ± 0.6	6.1 ± 0.3*	4.7 ± 0.3	3.1 ± 0.2*
<i>Postinjection</i>						
SO-T (<i>n</i> = 19)	184 ± 4	125 ± 1*	11.8 ± 0.5	6.3 ± 0.5*	4.2 ± 0.2	3.2 ± 0.3*
MI-V (<i>n</i> = 10)	167 ± 5	123 ± 2*	10.5 ± 0.6	5.4 ± 0.7*	4.4 ± 0.4	3.0 ± 0.3*
MI-GF (<i>n</i> = 12)	178 ± 2	123 ± 2*	12.0 ± 1.0	5.0 ± 0.6*	5.8 ± 0.8	2.7 ± 0.2*
MI-CPC (<i>n</i> = 11)	187 ± 4	128 ± 2*	11.0 ± 0.8	6.7 ± 0.8*	4.6 ± 0.4	2.8 ± 0.2*
MI-CPC + GF (<i>n</i> = 12)	188 ± 4	132 ± 2*	11.6 ± 1.0	5.4 ± 0.6*	5.1 ± 0.2	3.5 ± 0.4*

Values are means ± SE of: 1) R-R interval, 2) the SD of the mean R-R interval duration (SDRR), and 3) the root mean square of successive R-R interval square differences (r-MSSD), measured by telemetry ECG, before (Preinjection) and 15 days after treatment (Postinjection), in the different experimental groups. **P* < 0.05 significant differences vs. baseline values, within each group. SO, sham operation; MI, myocardial infarction; T, treatment; V, vehicle; GF, growth factor; CPC, cardiac progenitor cell.

of basic cardiac electrophysiological properties, namely CV, excitability, and refractoriness, as well as spatial dispersion of refractoriness. Epicardial recordings were further examined by phase maps (35) to evaluate the spatial distribution of inhomogeneity in conduction, which offers the possibility to detect areas of initial conduction block and correlates with the induction of reentrant arrhythmias.

CV-I was faster in MI-V group than SO-T, whereas CV-t was slower (+9% and -13%, respectively; *P* < 0.05) (Fig. 7, A and B). These changes were reversed by both CPC and CPC + GF administration (*P* < 0.05) with slightly larger effects of CPC + GF on CV-I (Fig. 7, A and B). Concomitantly, the high values of CV-I/CV-t anisotropy ratio in MI-V rats (+20% vs. SO-T), fell by about 15% in MI-CPC and matched SO-T values in MI-CPC + GF (Fig. 7C). Quite the opposite, MI-GF rats behaved similarly to MI-V, without any apparent effect of the treatment on in CV-I and CV-t alterations and, consequently, cardiac anisotropy, brought about by the ischemic injury. Of note, even small variations in propagation velocity are functionally important, as they reflect significant changes in cell-to-cell coupling attributable to the massive redundancy of gap junction-mediated intercellular communications (86).

In phase-mapping studies, the absolute inhomogeneity in conduction, described by percentile scores and expressed as *P*₅₋₉₅ (35), did not show any difference among groups at BCL (≈300 ms) (Fig. 7D). In contrast, the inhomogeneity independent of the average conduction velocity (*P*₅₋₉₅/*P*₅₀) was similarly increased in all treated and untreated MI animals (about 2-fold) compared with SO-T (Fig. 7E), suggesting that the

observed CV-I slowing against MI-V caused by CPCs and even more by CPCs + GFs (Fig. 7A) was not attributable to changes in local inhomogeneity.

Myocardial excitability was assessed by means of S-D curves and the related Rh and Chr values (see Fig. 4D). Roughly, Rh and Chr were respectively 20-fold and 2-fold greater in MI-V animals than SO-T (Fig. 7, F and G; *P* < 0.01), leading to a shift upward and to the right of S-D curves and hence a decline in cardiac excitability properties. In general, these changes were partially reverted by both CPCs and CPCs + GFs, whereas they were not affected by GFs alone, with the concomitant persistence of a high excitation threshold in MI-GF group.

The ERP trended to be slightly prolonged, and its dispersion was significantly increased by coronary ligation compared with SO-T (Fig. 7, H and I; *P* < 0.01). CPC and CPC + GF administration induced an additional ERP lengthening while reducing ERP dispersion, with comparable effects in the two animal groups (Fig. 7, H and I). GFs alone pushed ERP duration further up without any beneficial consequence on dispersion (Fig. 7, H and I).

Overall, data on basic cardiac electrophysiological properties indicated that CPCs and more so CPCs + GFs restored toward control values ventricular CV-I/CV-t anisotropy ratio enhanced by infarction, whereas the consequences of both treatments on cardiac excitability (partial recovery) and refractoriness (prolongation) were nearly alike. GFs alone increased ERP duration compared with MI-V as well as CPC and CPC + GF, without any significant impact on excitability and CV parameters.

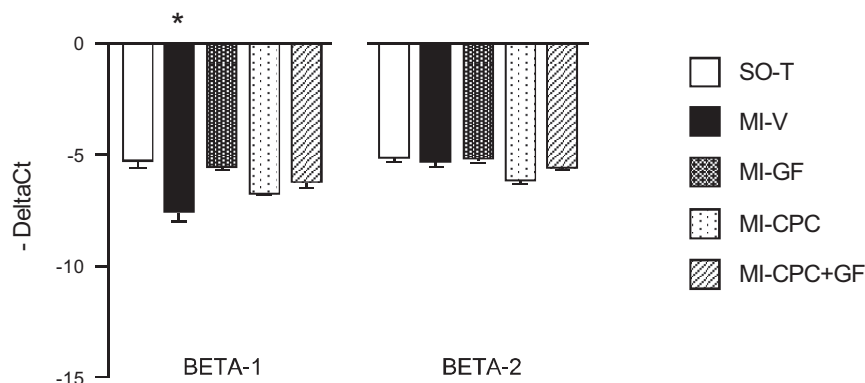


Fig. 6. Quantitative RT-PCR analysis. All treatments have similar effects on β -adrenergic receptor transcripts. Average values ± SE of $-\Delta C_t$, compared with cyclophilin, of mRNA levels for $\beta 1$ - (BETA-1) and $\beta 2$ - (BETA-2) adrenergic receptor isoforms, measured in the infarcted + peri-infarcted ventricular myocardium of MI-V (*n* = 2), MI-GF (*n* = 2), MI-CPC (*n* = 4), and MI-CPC + GF rats (*n* = 4), against SO-T (*n* = 4). Each bar represents the mean of the different samples, in technical triplicate. **P* < 0.05 vs. SO-T.

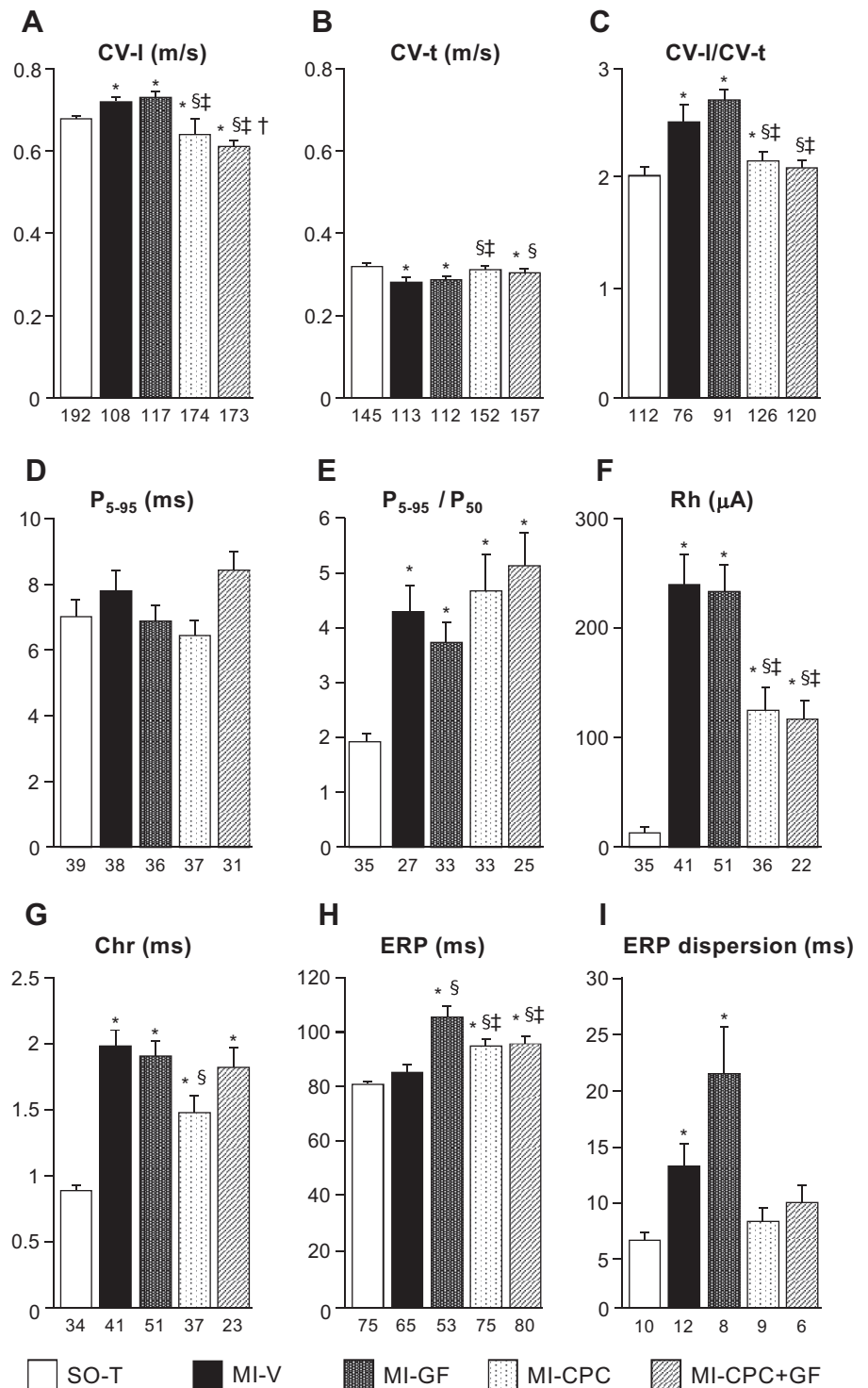


Fig. 7. Epicardial multiple-lead recording. GF and CPC + GF antiarrhythmic effects are mediated by different changes in cardiac electrophysiological properties. The following are shown: average values \pm SE of conduction velocity (CV) computed longitudinally (A: CV-l) and transversally (B: CV-t) to fiber orientation; anisotropy of CV (C: CV-l/CV-t); maximal difference in activation times (D: P₅₋₉₅), which expresses the absolute inhomogeneity in conduction; index of inhomogeneity (E: P₅₋₉₅/P₅₀), which expresses the spatial inhomogeneity in conduction independent of CV; rheobase (F: Rh); chronaxie (G: Chr); effective refractory period (H: ERP); and ERP dispersion (I). In each graph, the number of measurements is indicated under the bars. * $P < 0.05$ vs. SO-T; § $P < 0.05$ vs. MI-V; ‡ $P < 0.05$ vs. MI-GF; † $P < 0.05$ between MI-CPC and MI-CPC + GF.

Different Effects of Regenerative Treatments on Cellular and Molecular Determinants of Basic Cardiac Electrophysiological Properties and Vulnerability to Arrhythmias

It is generally recognized that local safe propagation of the impulse in cardiac tissue results from an optimal match between several variables, which also govern basic cardiac electrophysiological properties, such as cell-to-cell coupling, ex-

pression of ion channels, microscopic tissue structure, and cell morphology (31).

Gene expression analyses of cardiac connexins and ion channel subunits. In the infarcted + peri-infarcted area of untreated MI rat hearts, mRNA expression levels of Cx43 and channel proteins of the depolarizing ion currents I_{Na} (Na_v1.5) and $I_{Ca,L}$ (Ca_v1.2) and the repolarizing ion currents I_{to} (K_v4.2, K_v4.3, K_v1.4), I_{Kr} (K_v11.1), I_{Ks} (K_v7.1), and I_{K1} (K_{ir}2.1,

$K_{ir2.2}$) were markedly reduced compared with sham animals (range: $-20/-170\%$; $P < 0.05$; Fig. 8, A–E). On the contrary, Cx45 and Cx40 isoforms and channel subunit $Ca_v3.1$ were not affected by the ischemic damage, exhibiting equivalent values in SO-T and MI-V groups (Fig. 8, A and B). The lower expression of the various transcripts subsequent to coronary ligation was brought back toward sham values by one or more of the regenerative treatments, with the following significant

differences against MI-V group: 1) Cx43, $K_v11.1$, and $K_{ir2.2}$ transcripts were favorably influenced by all three regenerative therapies; 2) CPCs with GF adjunct had beneficial consequences on mRNA expression of $Ca_v1.2$, $K_v4.2$, and $K_v4.3$, whereas CPCs only did not; and 3) the salubrious effects of CPCs + GFs on $Ca_v1.2$ and $K_v4.2$ were shared by GFs alone, which also had a positive impact on $Na_v1.5$, $K_v1.4$, $K_v7.1$, and $K_{ir2.1}$. In summary, GFs taken individually partially restored

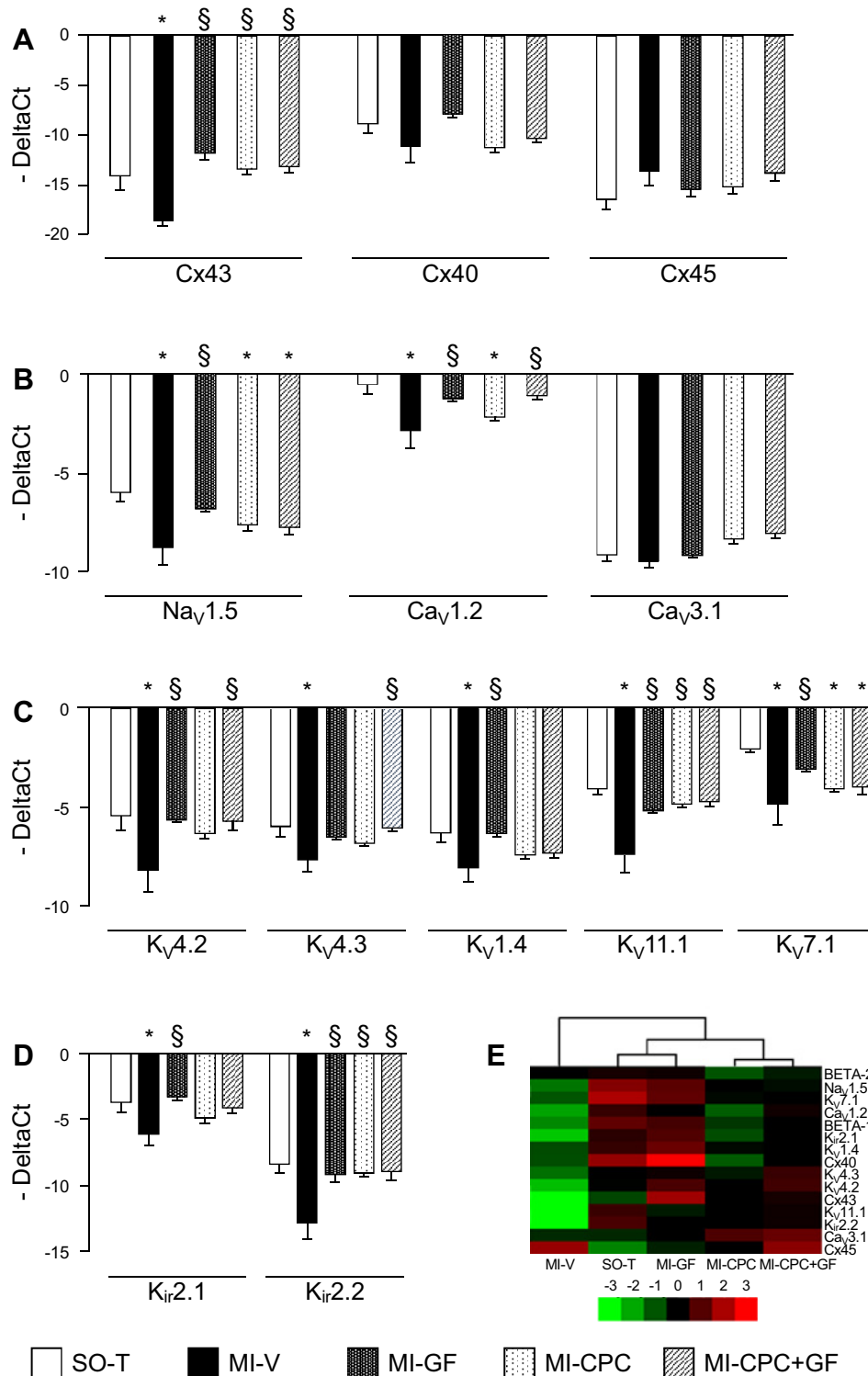


Fig. 8. Quantitative RT-PCR analysis: effects of regenerative treatments on connexin and ion channel isoforms. Average values \pm SE of $-\Delta Ct$, compared with cyclophilin, of mRNA levels for connexin and ion channel isoforms, measured in the infarcted + peri-infarcted ventricular myocardium of MI-V ($n = 2$), MI-GF ($n = 2$), MI-CPC ($n = 4$), and MI-CPC + GF ($n = 4$) rats, against SO-T ($n = 4$). Each bar represents the mean of the different samples, in technical triplicate. A: connexin-43 (Cx43), Cx40, and Cx45 isoforms. B: ion channel isoforms for depolarizing currents I_{Na} ($Na_v1.5$), $I_{Ca,L}$ ($Ca_v1.2$) and $I_{Ca,T}$ ($Ca_v3.1$). C and D: ion channel isoforms for repolarizing potassium currents I_{to} ($K_v4.2$, $K_v4.3$, and $K_v1.4$), I_{Kr} ($K_v11.1$), I_{Ks} ($K_v7.1$), and I_{K1} ($K_{ir2.1}$, $K_{ir2.2}$). E: heat map showing the Gene-wise mean-centered of $-\Delta Ct$ values of candidate genes labeled on the right. The heat map was clustered using centered correlation and Euclidean distance as the distance matrix for samples. Expression signals are converted into color. A 3-fold change is shown in red (increase) or in green (decrease) and no change in black. Color intensities are proportional to the variation of expression. * $P < 0.05$ vs. SO-T; § $P < 0.05$ vs. MI-V.

all transcripts except $K_v4.3$, whereas CPCs with GF adjunct had a more limited/specific action, suggesting that the two treatments differently cured the expression of transcripts deteriorated by the ischemic damage (Fig. 8, A–D). Importantly, as $Cx45$, $Ca_v3.1$, and $K_v1.4$ transcripts are mainly expressed in early stages of cardiac development, an increase during regenerative processes might be anticipated (1, 16, 85). Indeed, this was the case for $K_v1.4$, whereas $Cx45$ and $Ca_v3.1$ did not exhibit any sizeable difference among groups. However, in our experimental conditions, we could not exclude a possible masking effect on the two latter transcripts attributable to the overwhelming number of spare, mature myocytes in the infarcted area, opposite to newly formed myocytes.

Expression of $Cx43$ and $Cx40$ at protein level. It is known that during MI healing and scar formation, most action potentials of surviving myocytes in the border zone revert toward normal, highlighting the role of connexins as determinants of slow conduction and conduction block, necessary for reentry-mediated arrhythmias (91). Therefore, we further explored the expression of connexin isoforms, $Cx43$ and $Cx40$, in working myocytes of the adult heart at the protein level. Immunoblot assay documented that $Cx40$ and $Cx43$ expression in MI-V animals was approximately halved against SO-T (Fig. 9, A and B; $P < 0.01$). GF treatment with or without CPCs brought back toward control values the expression levels of both connexins, curing the negative impact of MI ($P < 0.05$), whereas CPCs alone did not (Fig. 9, A and B). Importantly, $Cx43$ expression roughly exhibited a similar behavior at mRNA and protein levels in the four MI experimental groups. On the contrary, the differences in $Cx40$ expression, which were unable to attain any statistical significance among groups by qRT-PCR, became clearly patent in immunoblot studies, suggesting a translational control of the corresponding gene. The above results were confirmed by immunofluorescence analysis, which generally documented similar trends of $Cx40$ and $Cx43$ changes in the various MI groups (Figs. 10 and 11), compared with Western blot ones, although the quantitative values and hence statistical significance in the two sets of data were only partly overlapping. This, however, was not surprising because of the methodological differences in immunoblot and immunofluorescence approaches.

Structural arrhythmogenic substrate: myocardial fibrosis and cell size. The amount of collagen accumulation, mostly in the form of diffuse interstitial and focal fibrosis, was barely detectable in SO-T animals and reached a value of about 2% of the remote myocardium in both treated and untreated MI hearts (MI-V: 1.82 ± 0.8 ; MI-GF: 1.32 ± 0.2 ; MI-CPC: 1.65 ± 0.1 ; MI-CPC + GF: 1.74 ± 0.1). In contrast, in the peri-infarcted myocardium, the three regenerative therapies reduced fibrotic damage by about 50% compared with MI-V (Fig. 12; $P < 0.01$). Finally, no significant differences were found among treated and untreated MI rat hearts in the hypertrophic response of spared cardiomyocytes, as measured by cross-sectional area (SO-T: $291.7 \pm 17.4 \mu m^2$; MI-V: 475.6 ± 15.3 ; MI-GF: 392.4 ± 19.3 ; MI-CPC: 441.9 ± 11.4 ; and MI-CPC + GF: 486.9 ± 18.2). As a result, myocardial fibrosis and cell size, which can modulate the impulse propagation in the heart with a major impact on its electrical stability, were similarly affected in all treated groups.

The finding that CPCs with or without GF adjunct and GFs alone have different consequences on cardiac electrical com-

petence prompted us to extend our observations to cardiac mechanics, anatomy, and regeneration.

Restoration of Cardiac Mechanical Function and Anatomy Was Equivalent in All Treated MI

LV mechanics. Marked signs of systolic and diastolic ventricular dysfunction developed in untreated MI-V animals against SO-T, including a significant increase in LVEDP ($+50\%$; $P < 0.05$), a reduction in $+dP/dt$ and $-dP/dt$, a prolongation of IVCT and IVRT, and an increase in the MPI (Table 4). In contrast, the ET showed comparable values among groups. Of note, the impairment of $+dP/dt$ and LVEDP in MI-V rats was significantly correlated with postmortem determination of infarct size (Fig. 13, A and B).

As a rule, the three regenerative treatments improved cardiac performance in a similar fashion, with a significant recovery of most hemodynamic parameters compared with MI-V (Table 4). Additionally, the correlations among deteriorated parameters and infarct size disappeared in MI-GF, MI-CPC, and MI-CPC + GF animals (Fig. 14, A–F), supporting the hypothesis that all regenerative therapies induced a parallel, partial recovery of ventricular mechanical performance, thus making cardiac function independent of the amount of tissue lost.

Cardiac anatomy. MI-V animals exhibited a significant dilation of LV chamber associated with a marked reduction in mass-to-chamber volume ratio (Fig. 15, A and B). The unfavorable anatomical remodeling following MI was reversed by GF, CPC, and CPC + GF administration in a similar fashion (Fig. 15, A and B). Concomitantly, all treatments had comparable effects on collagen deposition and cell size, as described above. Hence, by structural and anatomical data, the favorable effects of GFs, CPCs and CPCs + GFs on cardiac remodeling of the infarcted heart were equivalent.

Differential Influence of Treatments on Myocardial Repair

Engraftment of CPCs and formation of new functionally competent myocardium in MI-CPC and MI-CPC + GF hearts were documented by the presence of small, GFP^{pos}/α-SA^{pos} cardiomyocytes expressing $Cx43$ and $Cx40$ gap junctional proteins (Fig. 16, A and B). Quantification of these regenerative processes showed that, in the infarcted area, the density of GFP^{pos} cardiomyocytes was twofold higher in MI-CPC + GF than MI-CPC (Fig. 16; bar graph).

The effects of the injection of GFs, CPCs, or CPCs + GFs on cell proliferation were determined by analyzing BrdU incorporation in myocardial cells. All treatments had a positive impact on cardiomyocyte proliferation in the infarcted myocardium (Fig. 17, A–D). An increase up to 10-fold ($P < 0.05$) in DNA replication was measured in MI-GF, MI-CPC, and MI-CPC + GF rat hearts compared with untreated ones (Fig. 17; bar graph). Importantly, an additional marker of cycling cardiomyocytes, Ki-67, was simultaneously detected with BrdU labeling (Fig. 17, E–G).

Vasculogenesis in the infarcted area of treated animals was demonstrated by the presence of GFP^{pos} arterioles, attributable to CPC differentiation into α-SMA^{pos} cells, as well as GFP^{pos} capillary profiles (Fig. 18, A–D). To assess the differential impact of the three regenerative approaches on the recovery of myocardial perfusion, the cumulative arteriolar density was determined, indicating a significant comparable improvement

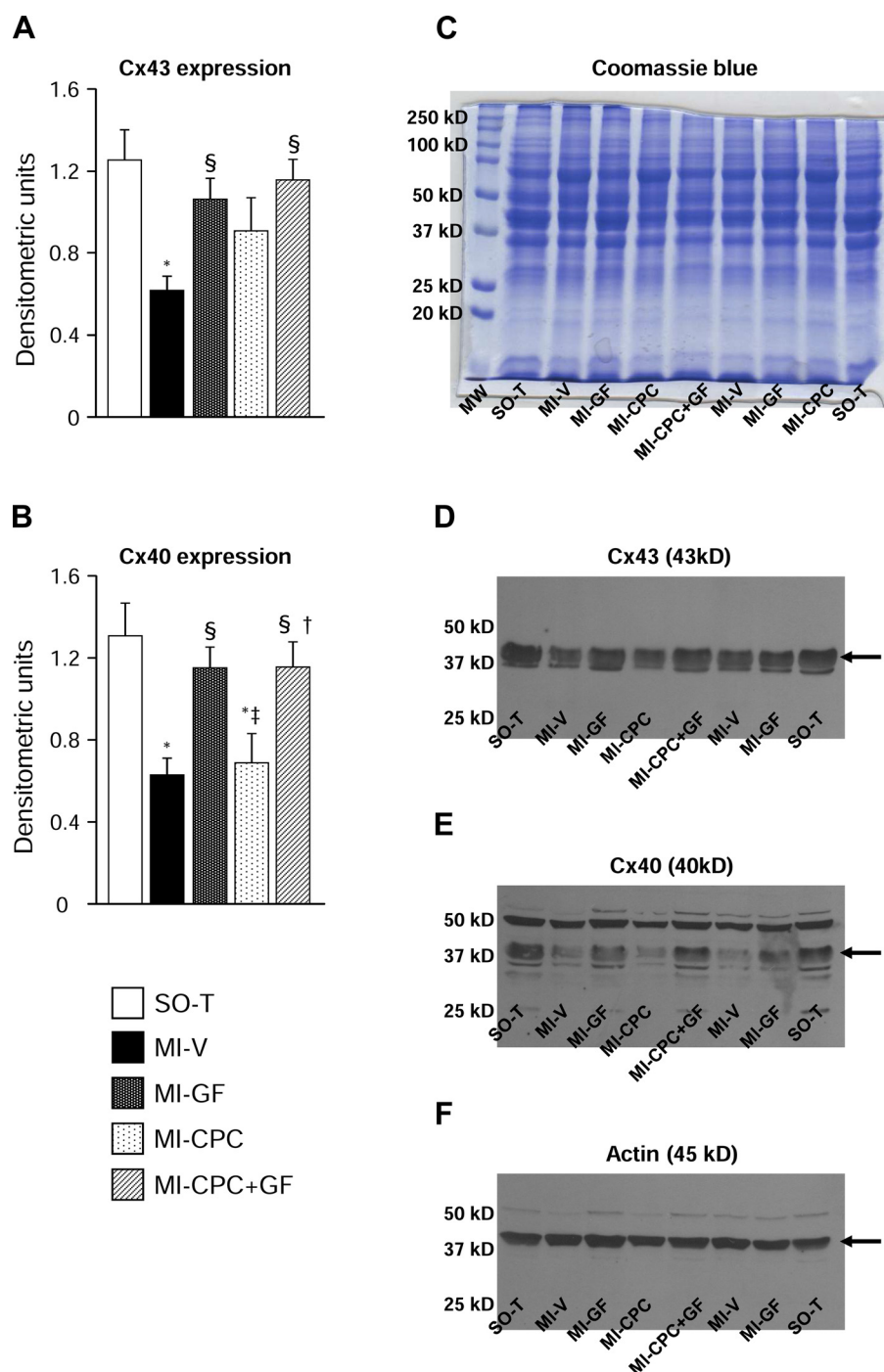


Fig. 9. Cx43 and Cx40 protein expression by immunoblot assay. Average values \pm SE of Cx43 (A) and Cx40 (B) protein expression, cumulatively measured in the infarcted + peri-infarcted areas of untreated (MI-V) and treated (MI-GF, MI-CPC, MI-CPC + GF) rat hearts, compared with SO-T. Data are expressed in densitometric units. Every bar represents the mean of 2–4 samples, in technical triplicate. Quantitative comparisons were performed on data derived from different gels processed in parallel (see MATERIALS AND METHODS). The visualization of all proteins in 1 gel stained with Coomassie blue is reported in C, together with the molecular weights. Examples of full-length blots for each connexin protein and internal control (actin) are shown in D–F, where arrows indicate the position of the relative bands. Polyclonal rabbit anti-Cx43/GJA1 (AB11370) and polyclonal rabbit anti-Cx40/GJA5 (AB101929) antibodies were used. * $P < 0.05$ vs. SO-T; § $P < 0.05$ vs. MI-V; ‡ $P < 0.05$ vs. MI-GF; † $P < 0.05$ between MI-CPC and MI-CPC + GF.

in all treated animals against MI-V (Fig. 18; bar graph). Similarly, the rarefaction of CD31/PECAM-1-labeled capillaries brought about by MI in the surviving myocardium (MI-V: $1,110 \pm 103$ n/mm²) was equally restored by all three repairing treatments (MI-GF: $1,527 \pm 109$ n/mm²; MI-CPC $1,305 \pm 155$; MI-CPC + GF $1,546 \pm 244$).

DISCUSSION

The present study demonstrates that, in the setting of chronic MI, local injection of CPCs with the addition of GFs is antiarrhythmic, largely restoring cardiac electrical viability

altered by ischemic injury, whereas CPCs alone do not have comparable, beneficial electrophysiological consequences. The ability of CPCs + GFs to ameliorate the electrogenesis of the mended heart was at least partly attributable to the recovery toward control values of cardiac anisotropy ratio CV-l/CV-t. This in turn was likely consequent to a parallel recovery of the expression levels of Cx43 and Cx40 isoforms as well as ion channel subunit Ca_v1.2, favorably affecting cardiomyocyte coupling and the spread of ventricular excitation. The injection of individual GFs reduced arrhythmias by less than CPCs + GFs. The better electrical function in MI-GF rats against

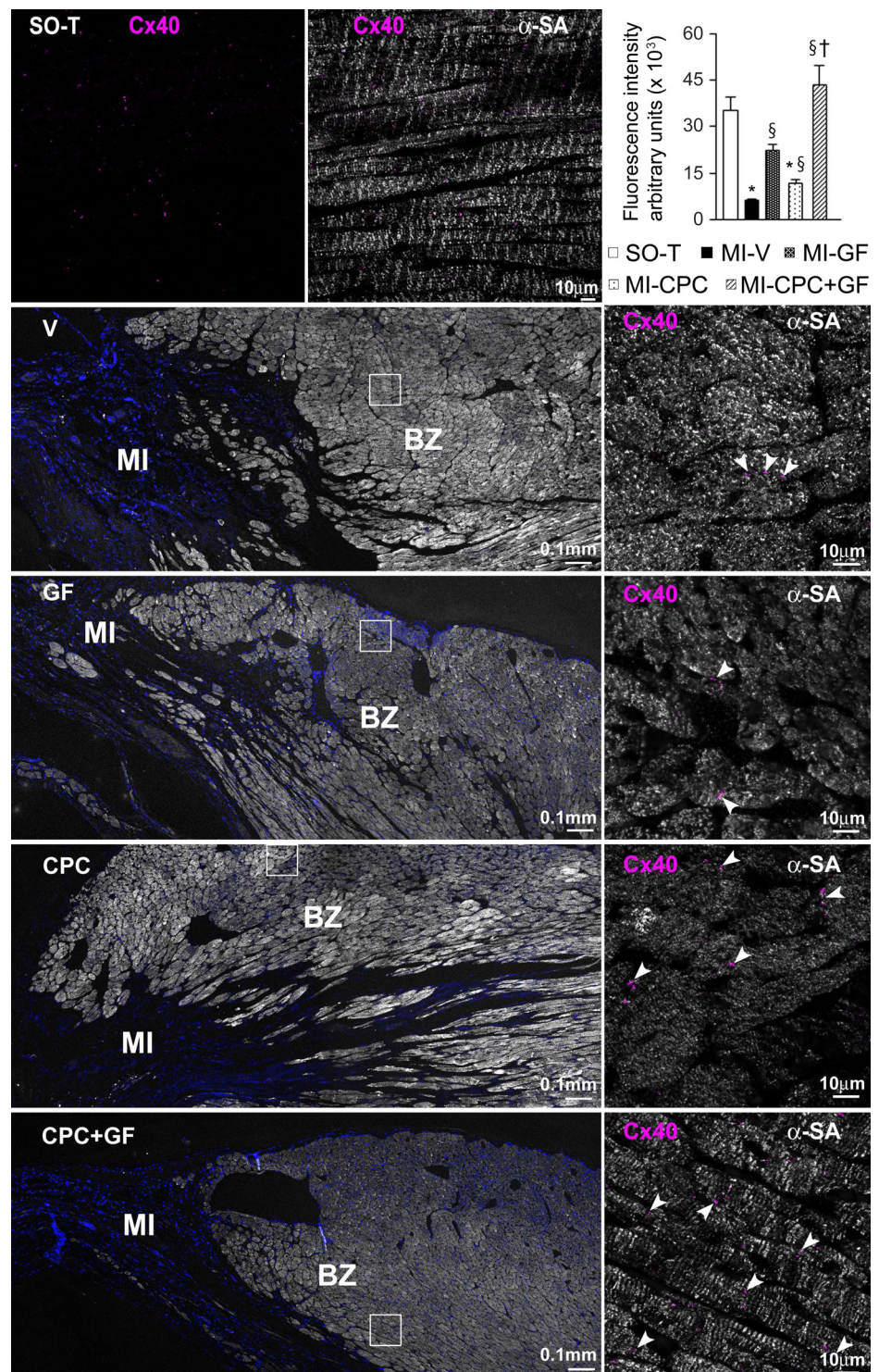


Fig. 10. Tissue analysis of the expression of Cx40 by immunofluorescence. Cx40 (magenta, arrowheads) labeling in sections of the SO-T LV and the infarcted myocardium (MI) and the border zone (BZ) from V-, GF-, CPC-, and CPC + GF-treated rat hearts. The area of the square in each MI panel is shown at higher magnification in the corresponding adjacent panel. Cardiomyocytes are labeled by α -sarcomeric actin (α -SA, white). Nuclei are shown by the blue fluorescence of DAPI. A scattered distribution of Cx40 immunofluorescence is present both in SO-T and infarcted myocardium. The quantification of cumulative Cx40 fluorescence intensity is reported in the bar graph (means \pm SE), for all animal groups. Polyclonal rabbit anti-Cx40/GJA5 (AB101929) antibody was used. * $P < 0.05$ vs. SO-T; $^{\S}P < 0.05$ vs. MI-V; $^{\dagger}P < 0.05$ between MI-CPC and MI-CPC + GF.

untreated MI appeared to result from a prolongation of ventricular refractoriness and was associated with a generalized recovery of most gap junctional and ionic channel proteins.

GF administration with or without CPCs resulted in an increased capacity of injected/resident CPCs to generate functionally competent myocardium within the infarct. The more robust repopulation of the damaged heart by newly formed appropriately connected myocytes might also have contributed to attenuation of cardiac electrical instability.

Decreased Proneness to Stress-Induced Arrhythmias and Autonomic Control

GF administration and still further CPC + GF significantly decreased the number of ventricular arrhythmias triggered by stress-mediated sympathetic stimulation, in conscious, freely moving animals. The duration of the recording epoch (a single 15-min recording), which may appear as a relatively short time window for appreciating baseline arrhythmic propensity, is a

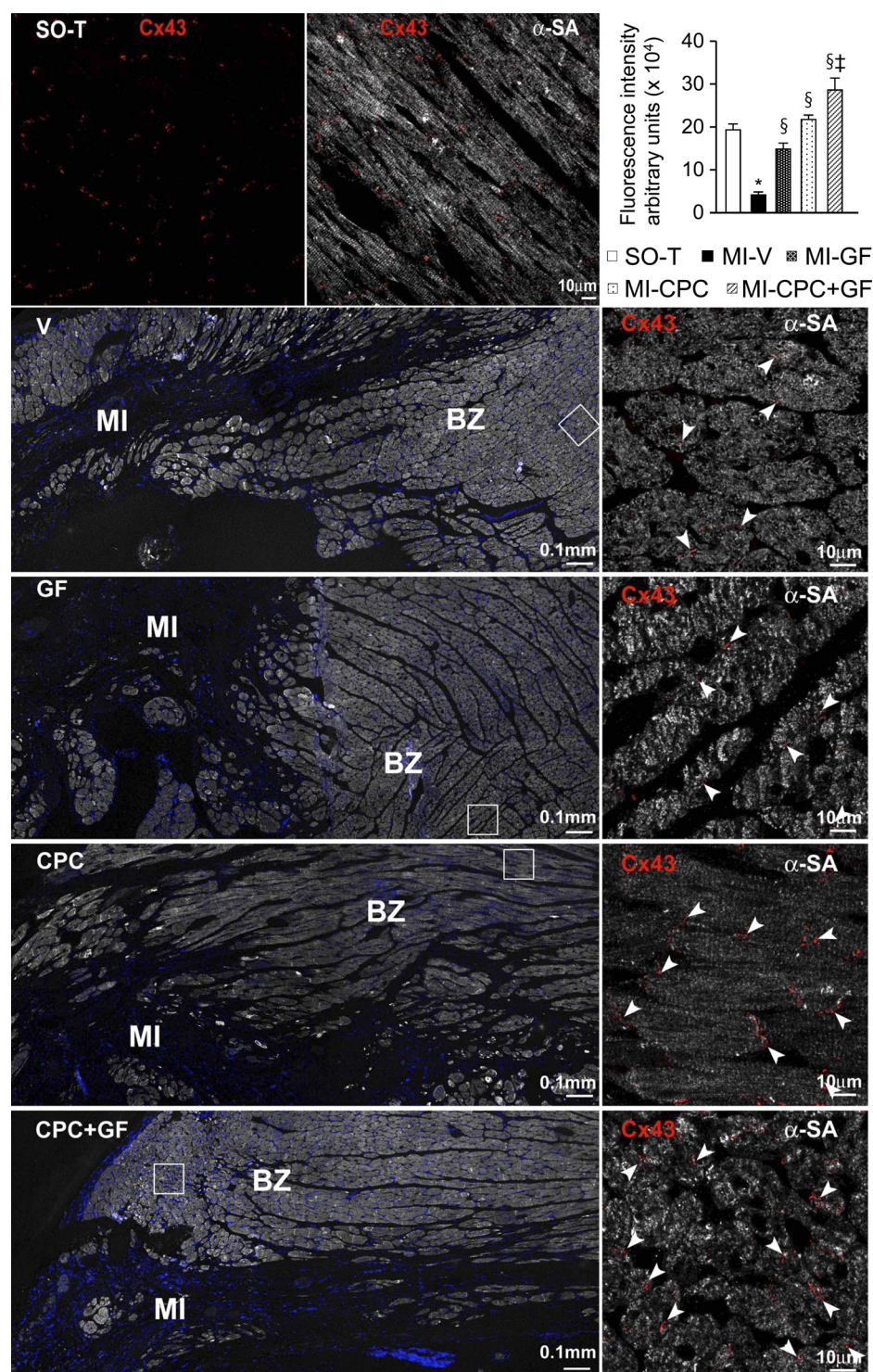
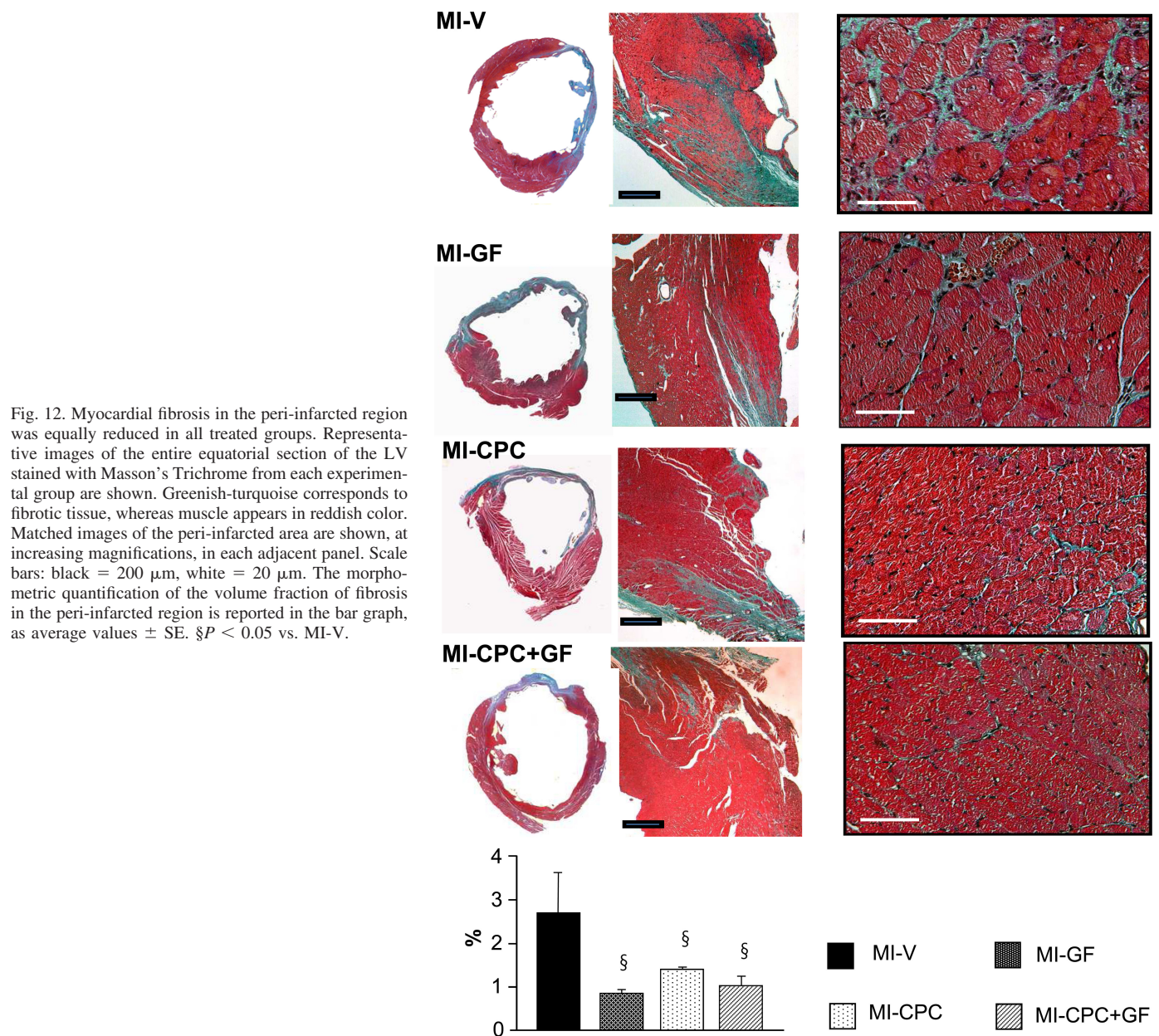


Fig. 11. Tissue analysis of the expression of Cx43 by Immunofluorescence. Cx43 (red, arrowheads) labeling in sections of the SO-T LV and the MI and the BZ from untreated and treated rat hearts. The prototypical end-to-end and side-by-side distribution of Cx43 is apparent in the longitudinally oriented myocardium from SO-T- and CPC-treated rats, while in obliquely/transversally oriented cardiomyocytes immunofluorescent signal of Cx43 appears more scattered. Polyclonal rabbit anti-Cx43/GJA1 (C6219) was used. Other explanations are as in Fig. 10. * $P < 0.05$ vs. SO-T; § $P < 0.05$ vs. MI-V; ‡ $P < 0.05$ vs. MI-GF.

rather validated methodology in the literature to establish stress-induced vulnerability to cardiac arrhythmic episodes within a given phase of the light/dark rhythm (70). Additionally, the enhanced sympathetic activity related to stress mimics circumstances encountered by social animals in everyday life, implying that our approach to induce arrhythmias by targeting the autonomic nervous system provides a more faithful representation of human clinical conditions (70). Published data (56) have indicated that mesenchymal stem cell therapy in a

swine model of MI can increase sympathetic nerve sprouting, with a potential arrhythmogenic effect. By contrast, in the same animal model, induced pluripotent stem cell transplantation ameliorated neural remodeling and reduced ventricular arrhythmias (92). In the present study, no significant difference in heart rate variability indexes was apparent among MI-GF, MI-CPC, and MI-CPC + GF groups. Similarly, lessening of LV β 1-adrenergic receptor transcripts following coronary occlusion was evenly restored toward control values by all three



regenerative therapies. Although we did not attempt a detailed investigation of adrenoceptor changes in untreated and treated MI, our data collectively suggest that lowered proneness to arrhythmias ensuing the injection of GF-supplemented CPCs and GFs alone was not attributable to changes in the autonomic input to the heart.

Impact of CPC and CPC + GF Administration on Basic Cardiac Electrophysiological Properties and Arrhythmogenic Substrate in Chronic MI

CPC repairing ability of cardiac electrical function was analyzed in terms of multicellular reentrant events rather than single-cell triggers. Indeed, data on the arrhythmogenic substrate of reentry at tissue level could represent important information, integrating single-cell results, which might be negatively influenced by the high degree of scattering of

measurements, given the heterogeneous properties of the scarred myocardium.

Conduction velocity and anisotropy ratio. Numerous reports indicate that, during post-MI ventricular healing, in surviving myocytes of the border zone, there is continued reduction of Cx43, bringing about a decrease in functional gap junction connections (91). Additional unfavorable effects on cell-to-cell contacts derive from fibrosis, which extends from the scar into viable border zones, mainly impairing transverse coupling (57). These alterations can attain sufficient magnitude to lessen conduction velocity and generate enhanced nonuniform anisotropy, thus causing severe ventricular arrhythmias via reentry mechanisms (86).

In most reports, the greater CV-l/CV-t anisotropy ratio in chronic MI is steadily linked to CV-t slowing, whereas CV-l contribution appears contradictory. This discrepancy was at-

Table 4. Hemodynamic measurements

	SO-T (n = 19)	MI-V (n = 10)	MI-GF (n = 16)	MI-CPC (n = 18)	MI-CPC + GF (n = 23)
LVSP, mmHg	111 ± 2.0	102 ± 4.6	105 ± 1.8	107 ± 1.6	106 ± 1.8
LVEDP, mmHg	5.3 ± 0.2	12.1 ± 1.1*	7.6 ± 0.3*§	8.4 ± 0.3*§	8.4 ± 0.4*§
+dP/dt, mmHg/s	8705 ± 213	5603 ± 373*	7008 ± 278*§	7090 ± 114*§	7037 ± 208*§
-dP/dt, mmHg/s	-5215 ± 36	-3984 ± 275*	-4650 ± 235	-4785 ± 106§	-4708 ± 154§
IVCT, ms	6.4 ± 0.2	13.5 ± 0.6*	10.7 ± 0.3*§	10.5 ± 0.4*§	8.7 ± 0.4*†‡§
IVRT, ms	7.5 ± 0.3	12.9 ± 0.2*	10.6 ± 0.7*§	9.7 ± 0.6*§	9.9 ± 0.4*§
ET, ms	66 ± 1.7	62 ± 2.7	69 ± 2.2	67 ± 1.6	65 ± 1.2
MPI	0.2 ± 0.01	0.4 ± 0.02*	0.3 ± 0.02*§	0.3 ± 0.02*§	0.3 ± 0.01*§

Values are means ± SE of left ventricular systolic pressure (LVSP), left ventricular end-diastolic pressure (LVEDP), maximum rate of ventricular pressure rise (+dP/dt), maximum rate of ventricular pressure reduction (-dP/dt), isovolumic contraction time (IVCT), isovolumic relaxation time (IVRT), ejection time (ET), and myocardial performance index (MPI). All treatments had a similar impact on cardiac mechanics. * $P < 0.05$ vs. SO-T; † $P < 0.05$ between MI-CPC and MI-CPC + GF groups; ‡ $P < 0.05$ vs. MI-GF; § $P < 0.05$ vs. MI-V.

tributed to a different balance in the various experimental conditions between the parameters, which determine conduction, including connexin-mediated cell coupling, sodium conductance, and tissue architecture (86). We found that enhanced anisotropy ratio in MI-V rats depended on slower CV-t associated with faster CV-l. Given that in spared cardiomyocytes of untreated MI hearts the cross-sectional area was about 1.5-fold greater than SO-T, the resulting changes in passive electrical properties would lead to a decline in intracellular longitudinal resistance, favoring electrical conduction along fibers and arguably contributing to accelerated CV-l (75).

It is generally recognized that MI hearts contain a complex mixture of cells participating in infarct healing, including fibroblasts, which express the gap junctional protein Cx43 (12) and, thereby, might have contributed to the changes in the same protein observed in our study. Although we did not perform a detailed immunophenotypic characterization of the cell populations participating in MI, one would expect that the cellular pattern associated with the ischemic injury was grossly equivalent in treated and untreated MI animals, suggesting a little involvement of fibroblast contribution in Cx43 differences among the four MI groups. In support of this conclusion, measurements of Cx43 immunofluorescence signals, excluding the areas occupied by interstitial fibroblasts and coronary vasculature, displayed differences among treated and untreated MI rat hearts qualitatively similar to immunoblot studies.

By our data, CPC and CPC + GF regenerative treatments brought back collagen deposition toward sham values, whereas a significant recovery of Cx43 expression against MI-V was

shown in the sole animals subjected to injection of GF-implemented CPCs. In accordance with classical literature (32), this difference might provide an explanation for the larger antiarrhythmic action of CPC + GF compared with CPC. Indeed, curing the unfavorable changes in both Cx43-mediated cell coupling and interstitial fibrosis would improve conduction velocity (18, 60), offsetting possible reentry pathways through the architectural structure of myocardial tissue. Nevertheless, we found a reduction rather than an increase of CV-l and CV-t in CPC + GF animals vs. CPC, suggesting that other arrhythmogenic substrates/mechanisms were positively influenced by GF adjunct to CPCs, favoring its distinctive antiarrhythmic action.

Current-to-load mismatch areas and spread of excitation in myocardial tissue. Altered impulse propagation in the heart can also derive from structural discontinuities associated with unique cellular architecture of myocardial tissue, where the size of a given excited region supplying depolarizing current (current source) is ill matched to the amount of depolarizing current necessary to excite the regions ahead (current sink or current load) (32, 36). In vitro studies documented that a small current source connected by gap junctions to a large current load can result in current-to-load mismatch that causes slowing of conduction velocity (62). Surprisingly, partial uncoupling confined to the load area can lead to a reduction of the load accelerating conduction, whereas partial recoupling can be followed by a decline in conduction, attributable to a novel increase in the load. In the latter conditions, the contribution of ionic Ca^{++} current is critically important for the success of

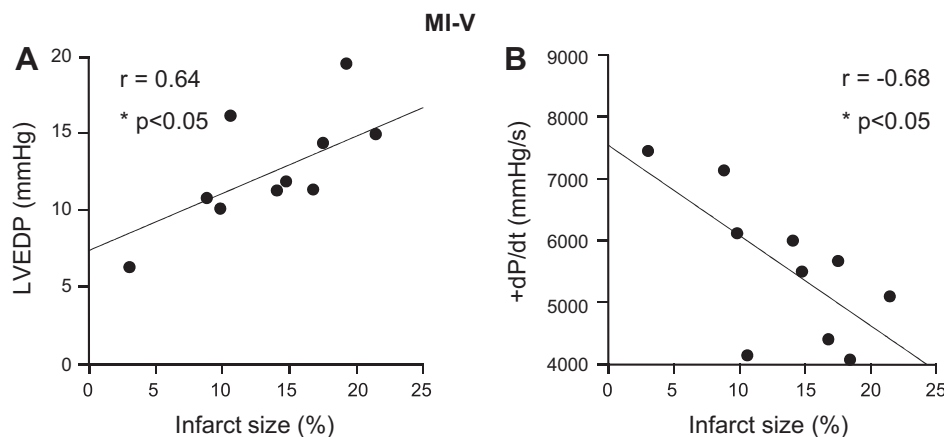


Fig. 13. The deterioration of LV performance is correlated with infarct size, in MI-V animals. Statistically significant ($*P < 0.05$) correlations between infarct size and LVEDP (A) and maximum +dP/dt (B), in MI-V group.

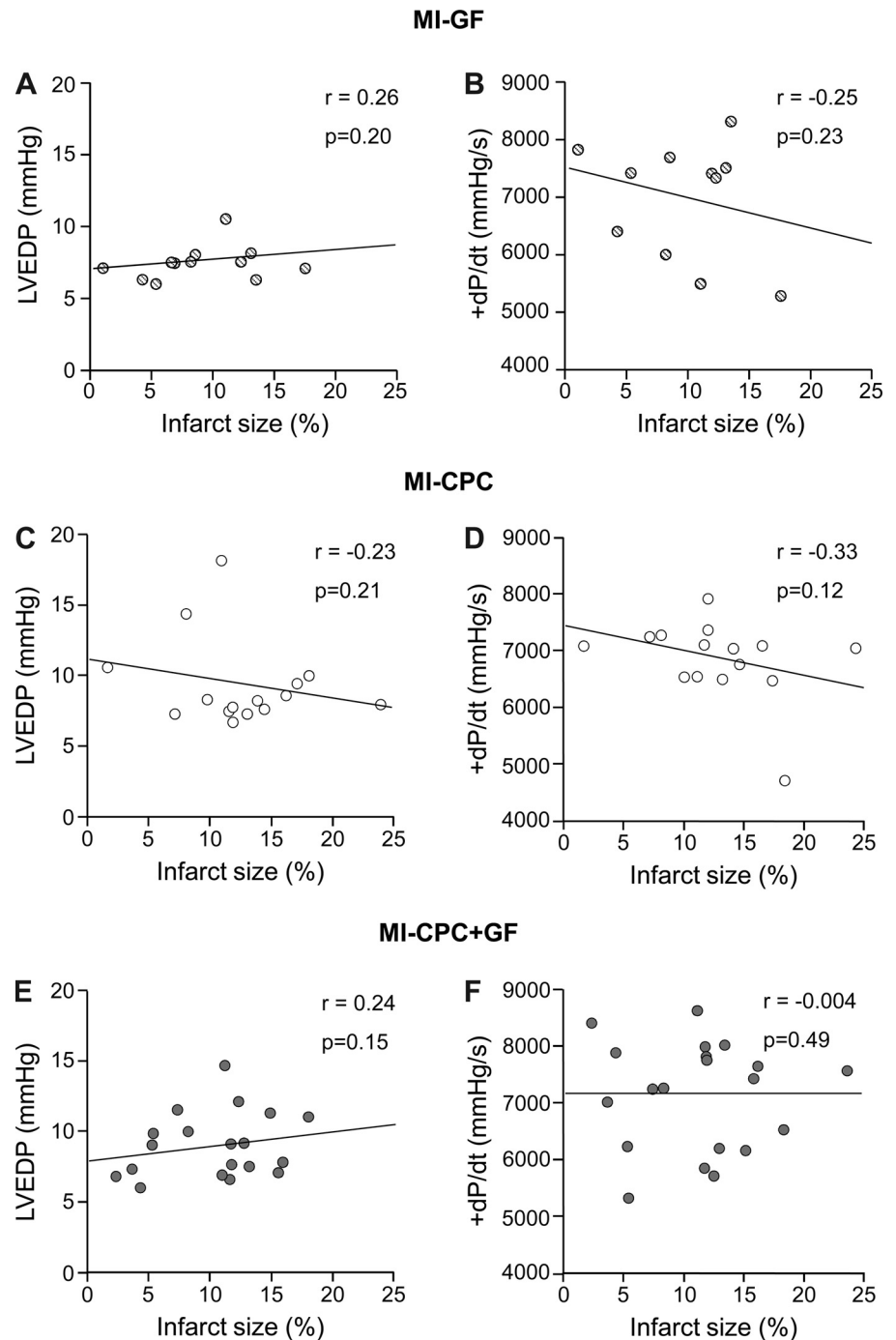


Fig. 14. LV hemodynamic function is independent of infarct size, in all treated MI groups. Linear correlations between infarct size and LVEDP and maximum $+dP/dt$, in MI-GF (A and B), MI-CPC (C and D), and MI-CPC + GF (E and F) animals. No correlation reaches statistical significance.

impulse propagation by sustaining depolarized transmembrane potentials, thereby increasing excitatory current flow to distant cells (61).

In the border zone of chronic MI, long known examples of current-to-load mismatch are portrayed by surviving strands of myocytes connected to larger regions of viable tissue (83). In our experimental settings, recovery of Cx43 expression promoted by regenerative treatments in such current mismatch zones was expected to induce partial recoupling, with decay in conduction velocity along fiber direction (CV-l) and further reduction of ventricular anisotropy ratio CV-l/CV-t, adding to the reduction caused by lower collagen deposition mentioned

above. However, CPC + GF treatment also increased the expression of $Ca_v1.2$ channel subunit at mRNA level and the related depolarizing current $I_{Ca,L}$ as likely expected outcomes, positively modulating impulse propagation, whereas CPCs alone did not. Therefore, the hypothesis is advanced that, in mismatch regions of the border zone, GF-implemented CPCs ameliorated intercellular connections while preventing an excessive decay in conduction velocity and blocks by a combined effect on the expression of Cx43 and ion channel subunit $Ca_v1.2$. These electrophysiological consequences could at least partly underlie the mechanisms of CPC + GF-mediated anti-arrhythmic action in the healed chronic MI.

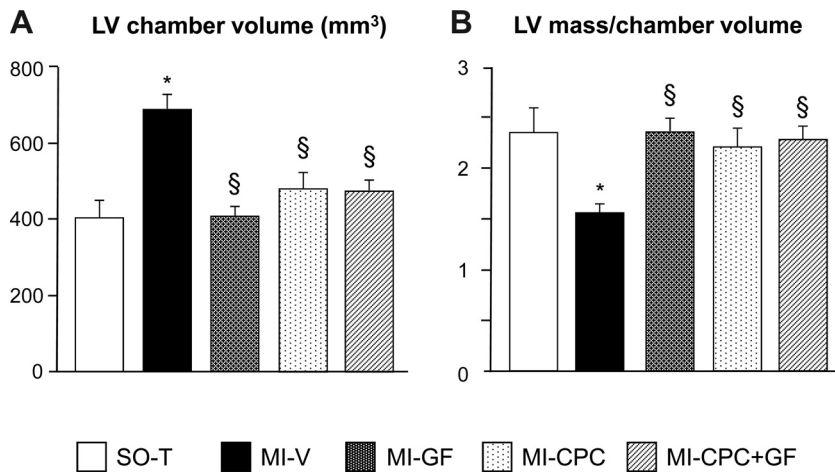


Fig. 15. Gross cardiac anatomy is equally restored by all regenerative treatments. Average values \pm SE of gross cardiac characteristics are as follows: LV chamber volume (A) and LV mass to chamber-volume ratio (B). * $P < 0.05$ vs. SO-T; § $P < 0.05$ vs. MI-V.

Furthermore, the Purkinje-fiber-ventricular junction represents another example for cardiac source-to-sink mismatch, where a small source (Purkinje fiber) is coupled to a large sink (mass of ventricular tissue) (55). Of note, downstream from the His bundle, the conduction system of most mammals, including rats, prominently expresses Cx40, which concurs in determining cellular connections at the Purkinje/working ventricular myocyte interface (69). So far, relatively little is known about how chronic MI influences expression of Cx40 and the consequent effects on spreading of excitation in the ventricular wall, although the importance of Cx40 in normal propagation has been recently emphasized (41). We found that Cx40 expression, markedly reduced in MI-V rat hearts, was significantly restored by GFs and CPCs combined. It is conceivable that, for a given recovery in $Ca_v1.2$ transcript, Cx40 mediated recoupling in Purkinje fiber-ventricular junction regions, deteriorated by infarction, impinged on cardiac electrogenesis in a way similar to recoupling accomplished by Cx43 in working myocardium, concurring with the enhancement of the antiarrhythmic action of CPC + GF administration.

Altogether, the favorable effect on cellular coupling and excitatory current flow, associated with restoring of Cx43, Cx40, and $Ca_v1.2$ expression in myocardial tissue, with or without structural discontinuities, appeared to be instrumental for the antiarrhythmic action of GF-implemented CPCs. Nevertheless, the effect of changes in cell-to-cell coupling and transmembrane Ca^{++} current cannot be considered independent of changes in other cellular/molecular determinants of arrhythmias mentioned above, similarly capable to affect electrical function in the highly interactive myocardial system. This will make it difficult to accurately predict the mechanisms of arrhythmogenesis and its prevention in any individual situation (32).

Excitability and refractoriness. Most measurements related to these electrophysiological properties exhibited comparable values in MI-CPC and MI-CPC + GF animals, suggesting a consequent minor role in the antiarrhythmic action of GF-implemented CPCs, despite the fact that we found several differences between the two regenerative treatments at the molecular level, which could influence both properties.

It is known that myocardial excitability is directly related to the total ionic inward current, which can exceed the repolarizing K current and myocyte cross-sectional area, and inversely

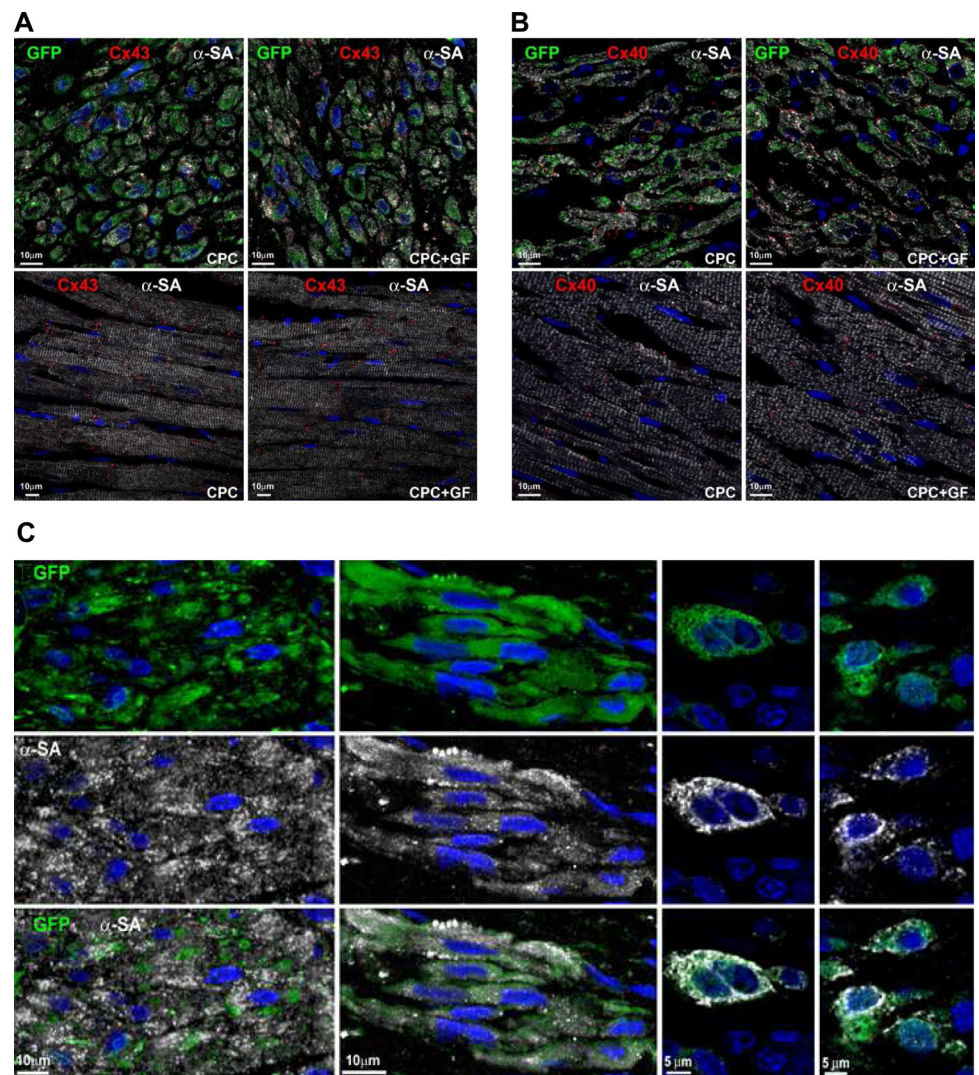
related to interstitial fibrosis and gap junction resistivity (31). In our study, the higher Rh and Chr values in MI-V rats than SO-T appeared to originate from the decline in total inward current as well as rise in collagen deposition and gap junction resistivity, which prevailed on the effects of the larger myocyte cross-sectional area. Rh and Chr changes were partially restored in a similar fashion by both regenerative treatments, notwithstanding the higher expression levels in MI-CPC + GF animals of $Ca_v1.2$, in addition to Cx40 and even more Cx43. This might not be surprising, as the positive influence of increased depolarizing current $I_{Ca,L}$ on the threshold for tissue excitation could be counteracted by the greater electric load originating from better intercellular connections promoted by the two connexins, mentioned above.

Ventricular refractoriness and much more its spatially non-uniform distribution were increased in MI-V group compared with sham, in accordance with most studies (13). Resetting of ERP dispersion to control values, induced by CPCs either alone or with GF adjunct, might be ascribed to the positive effects of both therapies on structural LV remodeling, helping to ameliorate the electrical stability of the regenerated heart. On the contrary, ERP persisted equally prolonged in MI-CPC and MI-CPC + GF animals regardless of the finding that only GF-implemented CPCs cured the decline of Cx40 and Cx43 transcripts induced by MI, while fostering mRNA expression of channel proteins of ion current $I_{Ca,L}$ ($Ca_v1.2$) and I_{to} ($K_v4.2$ and $K_v4.3$). However, ERP might be lengthened by the larger inward Ca^{++} current as well as connexin-mediated increased electrical load, and, on the other hand, it might be shortened by the enhanced outward K^+ current. Taken together, our data suggest that the effects of CPCs with and without GF adjunct on the determinants of ventricular refractoriness may result in complex interactions and require further investigations.

Different Electrophysiological Consequences of Locally Injected GFs Alone and in Combination with CPCs

Administration of GFs alone exerted salubrious effects on cardiac electrical competence of healed MI with a significant drop in propensity to arrhythmias, in support of our previous results (6). However, the arrhythmic risk in MI-GF rats was decreased to a lesser extent than MI-CPC + GF, and the better ventricular electrical stability in the two animal groups com-

Fig. 16. GF adjunct fosters CPC ability to regenerate the infarcted heart. *A* and *B*: representative confocal images of Cx43 (*A*; red spots) and Cx40 (*B*; red spots) immunofluorescence signals in sections of the infarcted (*top*) and spared (*bottom*) LV myocardium of CPC- (*A* and *B*, *left*) and CPC + GF-treated (*A* and *B*, *right*) hearts. Cardiomyocytes are recognized by the white fluorescence of α -SA. *A* and *B*, *top*: presence of small developing GFP^{pos} (green)/ α -SA^{pos} cardiomyocytes labeled by Cx40 and Cx43, respectively, documenting myocardial regeneration following the injection of GFP^{pos} CPCs. Blue fluorescence corresponds to DAPI staining of nuclei. Information on anti-Cx40 and anti-Cx43 antibodies is as in Figs. 10–11. *C*: sections of the infarcted myocardium from CPC + GF-treated rats documenting examples of newly formed GFP^{pos} (green)/ α -SA^{pos} (white) cardiomyocytes at increasing magnifications, from the left through the right panels. The 2 epitopes are separately shown in the upper and middle panels and merged in the lower panels. Blue fluorescence corresponds to DAPI staining of nuclei. The bar graph illustrates the quantification (means \pm SE) of GFP^{pos} cardiomyocytes, in MI-CPC and MI-CPC + GF hearts ($n = 6$ for each group). $\dagger P < 0.05$ between MI-CPC and MI-CPC + GF.



pared with MI-V appeared to result from different electrophysiological mechanisms. It has been long recognized that arrhythmias can be treated largely by modulating conduction velocity, or refractory period, or both (29). As mentioned above, GF-implemented CPCs reduced arrhythmia vulnerability by restoring toward control values ventricular CV-l/CV-t anisotropy ratio, at least partly attributable to a properly balanced resetting of Cx43, Cx40, and Ca_v1.2 expression (32, 61). On the contrary, the individual injection of GFs led to a remarkable increase of ERP, in the absence of any changes on conduction

velocity parameters compared with MI-V. This would prevent the occurrence of arrhythmias by prolonging the wavelength (i.e., the product of refractory period and CV) and eventually reducing the likelihood that a single or multiple reentrant circuit could originate in ventricular myocardium (87). Of note, this outcome was associated with a partial recovery of all but one of the transcripts deteriorated by the ischemic damage, suggesting a generalized, positive impact of GFs on most cellular/molecular determinants of cardiac electrogenesis. On the contrary, CPCs + GFs had a more targeted influence on the

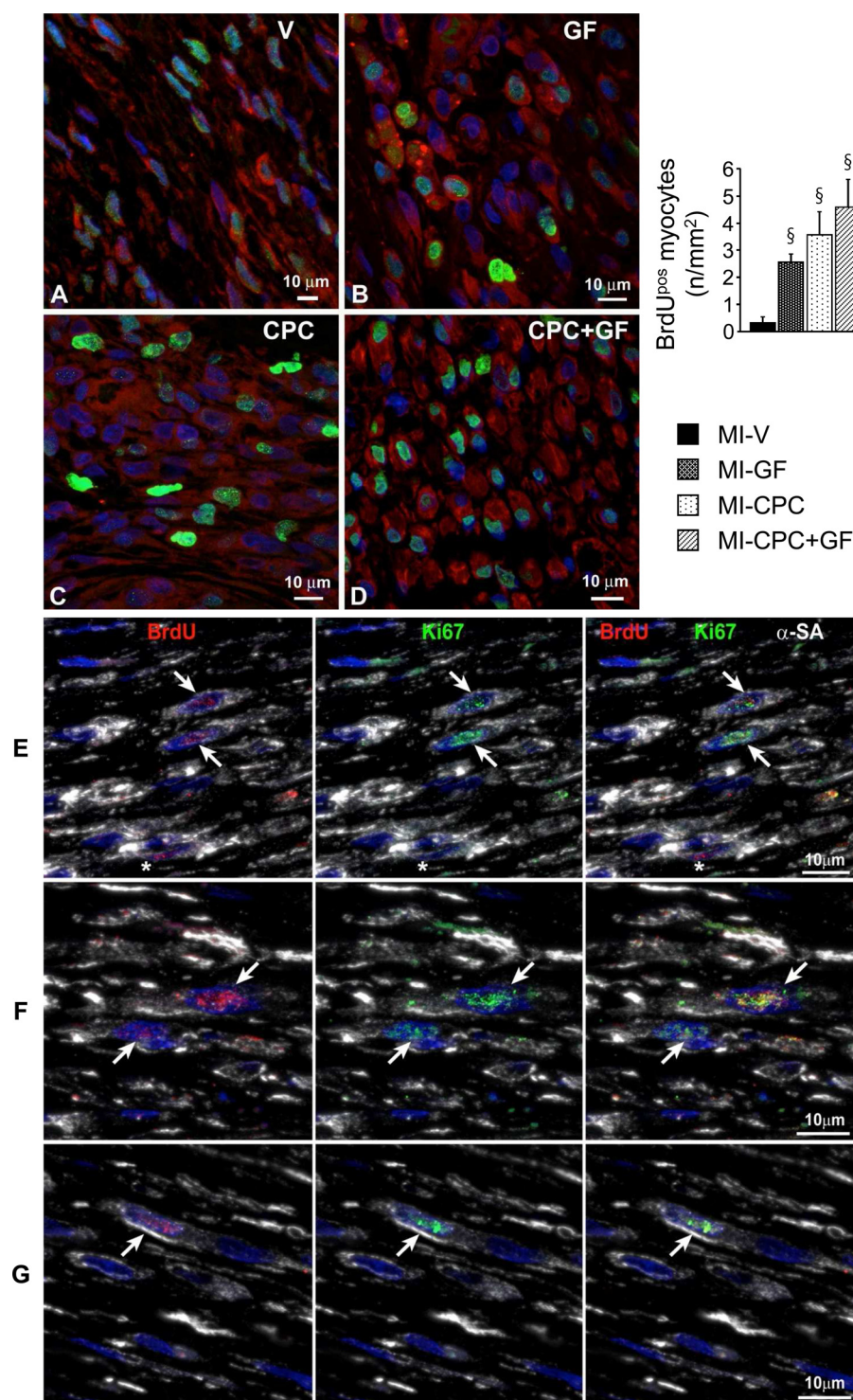


Fig. 17. Effect of regenerative approaches on cardiomyocyte proliferation. *A–D*: sections of untreated (V) and GF-, CPC-, and CPC + GF-treated infarcted myocardium, immunostained for 5-bromo-2'-deoxyuridine (BrdU) (green) and α -SA (red). BrdU^{pos} nuclei in small proliferating cardiomyocytes are apparent in all treated MI groups. *E–G*: sections of the myocardium from GF (*E*), CPC (*F*), and CPC + GF (*G*) rat hearts, subjected to triple immunolabeling BrdU (red fluorescence, *left*), Ki-67 (green, *middle*) and α -SA (white) antibodies. *Right*: nuclear coexpression of the 2 proliferative markers in α -SA^{pos} cardiomyocytes is documented in the merged panels of each experimental condition (white arrows). Asterisk points to a cell labeled by BrdU only. *A–G*: blue fluorescence corresponds to DAPI staining of nuclei. The quantification of BrdU labeling in cardiomyocytes is reported in the bar graph, as means \pm SE. $\S P < 0.05$ vs. MI-V.

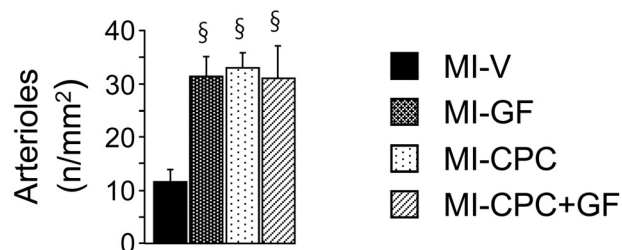
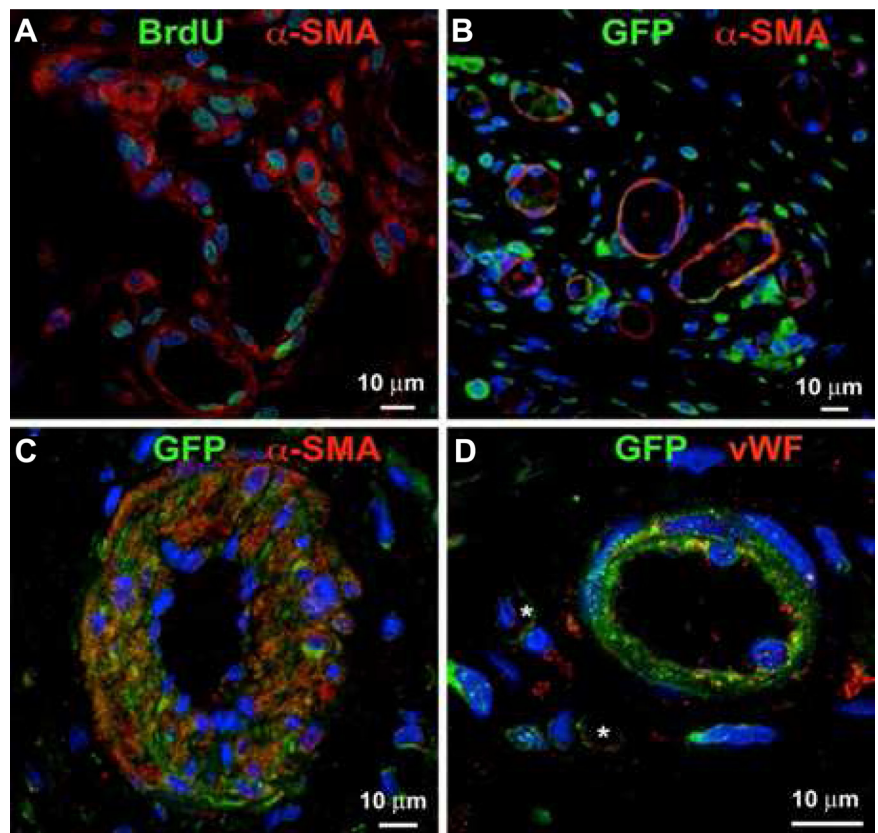
same determinants, which might be more capable to achieve an optimal match between them, as required for local safe changes in CV and hence propagation of the impulse (31). However, in accordance with the considerations made above on the effects of treatments on ERP, more work should be done to clarify how the numerous and in several instances opposite electrical influences, resulting from recovery of the various transcripts mediated by GFs, complemented each other. Also, it remains to be established how these influences led to the excitability/

refractoriness changes in GF animals documented in our study, including the persistence of high ERP dispersion.

Cx40 Expression in Ventricular Myocytes

Immunofluorescence and immunoblot data documenting the presence of Cx40 isoform in SO-T rat ventricles were unexpected because there is no published experimental evidence of a robust expression of this protein in normal

Fig. 18. Effect of regenerative approaches on vasculogenesis. *A*: proliferating arterioles are documented by BrdU (green)-labeled nuclei of α -smooth muscle actin (α -SMA, red)-positive cells. *B*: section of the infarcted area from a CPC-treated heart in which vasculogenesis is documented by α -SMA^{pos} vascular profiles, also labeled by GFP (green). Numerous GFP^{pos}/ α -SMA^{neg} cells not organized in vascular structures are present as well. *C*: cross section of a GFP^{pos}/ α -SMA^{pos} resistance arteriole from a CPC + GF-treated heart is shown at high magnification. *D*: GFP^{pos} (green)/von Willebrand factor (vWF^{pos}) (red) endothelial cells in capillaries (*) and luminal aspect of an arteriolar profile (center image) are shown. *A–D*: blue fluorescence corresponds to DAPI staining of nuclei. The quantification of arteriolar density is reported in the bar graphs, as means \pm SE. $\S P < 0.05$ vs. MI-V.



adult, working ventricular cardiomyocytes. However, SO-T animals along with treated and untreated MI rats were subjected to several experimental procedures with an outcome on ventricular structural properties representing a situation different from a normal condition. As summarized in Fig. 2, these procedures included the following: 1) three successive thoracotomies, with damage/removal of ventricular pericardium and predictable myocardial involvement; 2) microsurgery for coronary ligation or equivalent SO; and 3) intramyocardial injections for delivering specific treatments or vehicle. Moreover, positioning of the electrode grid at the ventricular surface in epicardial recording experiments generated injury currents at each electrode site lasting for about 30 min (40), indicative of a local damage. In general, one can anticipate that, by the above maneuvers, some degree of cell death occurred in ventricular myocardium of SO-T rats, conceivably followed by reactive cellular hypertrophy. Despite that Cx40 is less intensively characterized compared with Cx43 (65), studies in hypertensive rats demonstrated a 3.1-fold increase in Cx40 expression

compared with normal myocardium, during the early stage of hypertrophic remodeling (3). Similar results were obtained in explanted hearts from transplant patients with end-stage HF attributable to ischemic cardiomyopathy (20). In both cases, the elevated Cx40 expression correlated with an increased depth of Cx40-expressing myocytes consistent with differentiation of working myocytes adjacent to Purkinje cells, developing conduction myocyte-type properties (20). Alternatively, the changes have been attributed to expansion of the Purkinje system (68). This cellular substrate can provide an explanation for the sizeable Cx40 expression documented in our studies in SO-T rat hearts. The ensuing differences among groups were likely resulting from the distinctive impact of GF, CPC, and CPC + GF reparative treatments on the same substrate. Further complexity may be expected in the various MI groups against SO-T, deriving from reactive hypertrophy associated with the presence of scarred myocardial tissue and border zone areas, and, in treated MI rats, newly formed cardiomyocytes likely belonging to both working and conductive tissue.

Cardiac Regeneration, Anatomy, and Mechanics

Chronic myocardial damage negatively conditions the activation, migration, and growth of CPCs, ultimately controlling the regenerative response of the pathological heart. It has been assumed that the loss of a chemokine/GF gradient within the healed myocardium may be responsible for the lack of endogenous repair despite an actual increase of tissue CPCs (58, 64, 82). Our results on BrdU incorporation and Ki-67 labeling support the contention that more robust myocardial regeneration, compared with untreated MI, can be obtained via all three regenerative therapies, which may reverse the unfavorable microenvironment and promote the repairing ability of CPCs either resident or locally injected.

Information obtained in GFP^{POS} CPC experiments indicated that GF adjunct favors CPC differentiation, resulting in more numerous Cx43- and Cx40-labeled cardiomyocytes within the infarcted area and at the border zone. These newly formed, electrically connected cells may represent a further mechanism of the observed reduction in ventricular arrhythmic events mediated by CPCs + GFs. By these findings, GF-induced control of the expression of different types of connexins within the regenerated infarct offers an exciting explanation of the beneficial effects of the proposed repairing approach.

All regenerative treatments used in the present study were able to rescue, anatomically and mechanically, the infarcted heart. On the contrary, a divergent behavior was found between the overt positive consequences on electrical stability produced by GFs and further more CPCs + GFs and the lack of parallel, additional recovery in cardiac mechanics and anatomy against CPCs alone. To date, no consensus exists on whether the repairing process mediated by CPCs as well as other stem cell populations in the infarcted heart results from direct or indirect mechanisms, i.e., differentiation of transplanted stem cells or paracrine factors secreted by the same cells (22, 23, 67, 84). In keeping with the first hypothesis, the documented discrepancy of effects on cardiac mechanical and electrical properties might be linked to the fact that, although more contractile cells were generated within the infarct by GFs as well as CPCs + GFs compared with CPCs only, the fully mature phenotype of newly formed cardiomyocytes was not achieved. In accordance with our previous observations, the volume of cardiomyocytes generated 2–3 wk after injection of rat or human CPCs (4, 5, 80), GFs (6, 82), or CPCs + GFs (63, 64) ranges on average from 2,000 to 5,000 μm^3 and does not reach that of adult cells ($\approx 25,000 \mu\text{m}^3$). Thus, it is conceivable that these regenerative processes, although advantageous, could not impact on detectable differences among treatments in the improvement of gross anatomic remodeling and global cardiac mechanics. Alternatively, by the “paracrine hypothesis” (26), the better electrical performance in animals treated with GFs and, increasingly more, GF-supplemented CPCs vs. sole CPCs should depend on a complementary/synergistic role played by HGF and IGF-1 and their receptors, as important intermediates of cell-to-cell signaling, possibly related to the degree of CPC availability. In this case, our findings might suggest that HGF/IGF-1-mediated paracrine effects on cardiac function are more committed to restore the electrical than the mechanical and structural properties. Furthermore, the paracrine mechanisms involved appear to be different, depending on whether GFs were injected individually or in adjunct to CPCs, with a prevailing positive

impact on cardiac refractoriness in the former case and conduction velocity in the latter. However, such an explanation requires additional complex experimental approaches.

Conclusions

Combined strategies that promote robust myocardial regeneration, local intercellular coupling, and ion channel reorganization ensue more efficient functional post-MI recovery. Further investigations are necessary to deeply understand the molecular and genetic mechanisms of the antiarrhythmic effect of GF adjunct in stem cell-mediated cardiac repair, as well as to exploit the potential of myocardial plasticity in restoring the multiple functional aspects of ischemic cardiomyopathy.

ACKNOWLEDGMENTS

The authors thank Prof. Aderville Cabassi for the critical review of the manuscript and advice in analysis of adrenoceptor data. The authors also thank Emilia Corradini for the invaluable technical assistance in histological preparations and Gabriella Becchi for support to immunohistochemical studies.

GRANTS

This study was supported by the following grants: European Commission CORDIS FP7-BIOSCENT, NMP-214539 2007, Italian Ministry of Education, University and Research MIUR 2007AL2YNC, Italian Ministry of Health THEAPPL 2008, Young Researcher Project, Italian Ministry of Health Grant No. GR-2009-1530528, and funding by “Fondazione Cassa di Risparmio di Parma,” and “Istituto Nazionale di Ricerche Cardiovascolari.”

DISCLOSURES

No conflicts of interest, financial or otherwise, are declared by the authors.

AUTHOR CONTRIBUTIONS

M.S., L.B., S.R., C.F., G.G., C.L., M.M., E.D.P., G.G.S., G.M., K.U., and A.D.A. performed experiments; M.S., L.B., S.R., C.F., G.G., C.L., M.M., E.D.P., G.G.S., G.M., K.U., A.D.A., and E. Musso analyzed data; M.S., L.B., S.R., C.F., G.G., C.L., M.M., G.M., K.U., A.D.A., E. Macchi, D.S., F.Q., and E. Musso interpreted results of experiments; M.S., L.B., C.F., E.D.P., G.G.S., and K.U. prepared figures; M.S., L.B., S.R., C.F., G.G., C.L., M.M., E.D.P., G.G.S., G.M., K.U., A.D.A., E. Macchi, D.S., F.Q., and E. Musso approved final version of manuscript; M.M., D.S., F.Q., and E. Musso drafted manuscript; E. Macchi, D.S., F.Q., and E. Musso conception and design of research; E. Macchi, D.S., F.Q., and E. Musso edited and revised manuscript.

REFERENCES

- Alcoléa S, Théveniau-Ruissy M, Jarry-Guichard T, Marics I, Tzouanacou E, Chauvin JP, Briand JP, Moorman AFM, Lamers WH, Gros DB. Downregulation of Connexin45 gene products during mouse heart development. *Circ Res* 84: 1365–1379, 1999.
- Bastide B, Neyses L, Ganten D, Paul M, Willecke K, Traub O. Gap junction protein Connexin40 is preferentially expressed in vascular endothelium and conductive bundles of rat myocardium and is increased under hypertensive conditions. *Circ Res* 73: 1138–1149, 1993.
- Bartunek J, Behfar A, Dolatabadi D, Vanderheyden M, Ostojic M, Dens J, El Nakadi B, Banovic M, Beleslin B, Vrolix M, Legrand V, Vrints C, Vanoverschelde JL, Crespo-Diaz R, Homsey C, Tendera M, Waldman S, Wijns W, Terzic A. Cardiopoietic stem cell therapy in heart failure: the C-CURE (Cardiopoietic stem Cell therapy in heart failure) multicenter randomized trial with lineage-specified biologics. *J Am Coll Cardiol* 61: 2329–2338, 2013. (Corrigendum. *J Am Coll Cardiol* 62: 2457–2458, 2013).
- Bearzi C, Rota M, Hosoda T, Tillmanns J, Nascimbene A, De Angelis A, Yasuzawa-Amano S, Trofimova I, Siggins RW, Lecapitaine N, Cascapera S, Beltrami AP, D'Alessandro DA, Zias E, Quaini F, Urbanek K, Michler RE, Bolli R, Kajstura J, Leri A, Anversa P. Human cardiac stem cells. *Proc Natl Acad Sci USA* 104: 14068–14073, 2007.
- Beltrami AP, Barlucchi L, Torella D, Baker M, Limana F, Chimenti S, Kasahara H, Rota M, Musso E, Urbanek K, Leri A, Kajstura J,

- Nadal-Ginard B, Anversa P. Adult cardiac stem cells are multipotent and support myocardial regeneration. *Cell* 114: 763–776, 2003.
6. Bocchi L, Savi M, Graiani G, Rossi S, Agnelli A, Stilitano F, Lagrasta C, Baruffi S, Berni R, Frati C, Vassalle M, Squarcia U, Cerbai E, Macchi E, Stilli D, Quaini F, Musso E. Growth factor-induced mobilization of cardiac progenitor cells reduces the risk of arrhythmias, in a rat model of chronic myocardial infarction. *PLoS One* 6: e17750, 2011.
 7. Bolli R, Chugh AR, D'Amario D, Loughran JH, Stoddard MF, Ikram S, Beache GM, Wagner SG, Leri A, Hosoda T, Elmore JB, Goihberg P, Cappelletta D, Solankhi NK, Fahsah I, Rokosh DG, Slaughter MS, Kajstura J, Anversa P. Cardiac stem cells in patients with ischaemic cardiomyopathy: initial results of the SCPIO trial. *Lancet* 378: 1847–1857, 2011.
 8. Bristow MR, Ginsburg R, Umans V, Fowler M, Minobe W, Rasmussen R, Zera P, Menlove R, Shah P, Jamieson S, Stinson EB. Beta 1- and beta 2-adrenergic-receptor subpopulations in nonfailing and failing human ventricular myocardium: coupling of both receptor subtypes to muscle contraction and selective beta 1-receptor down-regulation in heart failure. *Circ Res* 59: 297–309, 1986.
 9. Brodde OE. Beta 1- and beta 2-adrenoceptors in the human heart: properties, function, and alterations in chronic heart failure. *Pharmacol Rev* 43: 203–242; 350, 1991.
 10. Brunel N, van Rossum MCW. Quantitative investigations of electrical nerve excitation treated as polarization. *Biol Cybern* 97: 341–349, 2007.
 11. Cai B, Wang G, Chen N, Liu Y, Yin K, Ning C, Li X, Yang F, Wang N, Wang Y, Pan Z, Lu Y. Bone marrow mesenchymal stem cells protected post-infarcted myocardium against arrhythmias via reversing potassium channels remodelling. *J Cell Mol Med* 18: 1407–1416, 2014.
 12. Camelliti P, Devlin GP, Matthews KG, Kohl P, Green CR. Spatially and temporally distinct expression of fibroblast connexins after sheep ventricular infarction. *Cardiovasc Res* 62: 415–425, 2004.
 13. Carmeliet E, Vereecke J. *Cardiac Cellular Electrophysiology*. Dordrecht, the Netherlands: Kluwer Academic, 2002, p. 307–330.
 14. Chamuleau SA, Vrijnsen KR, Rokosh DG, Tang XL, Piek JJ, Bolli R. Cell therapy for ischaemic heart disease: focus on the role of resident cardiac stem cells. *Neth Heart J* 17: 199–207, 2009.
 15. Chen HS, Kim C, Mercola M. Electrophysiological challenges of cell-based myocardial repair. *Circulation* 120: 2496–2508, 2009.
 16. Chen X, Wilson RM, Kubo H, Berretta RM, Harris DM, Zhang X, Jaleel N, MacDonnell SM, Bearzi C, Tillmanns J, Trofimova I, Hosoda T, Mosna F, Cribbs L, Leri A, Kajstura J, Anversa P, Houser SR. Adolescent feline heart contains a population of small, proliferative ventricular myocytes with immature physiological properties. *Circ Res* 100: 536–544, 2007.
 17. Chong JJ, Yang X, Don CW, Minami E, Liu YW, Weyers JJ, Mahoney WM, Van Biber B, Cook SM, Palpant NJ, Gantz JA, Fugate JA, Muskheli V, Gough GM, Vogel KW, Astley CA, Hotchkiss CE, Baldessari A, Pabon L, Reinecke H, Gill EA, Nelson V, Kiem HP, Laflamme MA, Murry CE. Human embryonic-stem-cell-derived cardiomyocytes regenerate non-human primate hearts. *Nature* 510: 273–277, 2014. (Corrigendum. Corrected online June 11, 2014).
 18. de Jong S, van Veen TA, van Rijen HV, de Bakker JM. Fibrosis and cardiac arrhythmias. *J Cardiovasc Pharmacol* 57: 630–638, 2011.
 19. Dodge HT, Baxley WA. Left ventricular volume and mass and their significance in heart disease. *Am J Cardiol* 23: 528–537, 1969.
 20. Dupont E, Matsushita T, Kaba RA, Vozzi C, Coppen SR, Khan N, Kaprielian R, Yacoub MH, Severs NJ. Altered connexin expression in human congestive heart failure. *J Mol Cell Cardiol* 33: 359–371, 2001.
 21. Ellison GM, Torella D, Dellegrataglie S, Perez-Martinez C, Perez de Prado A, Vicinanza C, Purushothaman S, Galuppo V, Iaconetti C, Waring CD, Smith A, Torella M, Cuellas Ramon C, Gonzalo-Orden JM, Agosti V, Indolfi C, Galianes M, Fernandez-Vazquez F, Nadal-Ginard B. Endogenous cardiac stem cell activation by insulin-like growth factor-1/hepatocyte growth factor intracoronary injection fosters survival and regeneration of the infarcted pig heart. *J Am Coll Cardiol* 58: 977–986, 2011.
 22. Ellison GM, Vicinanza C, Smith AJ, Aquila I, Leone A, Waring CD, Henning BJ, Stirparo GG, Papait R, Scarfò M, Agosti V, Viglietto G, Condorelli G, Indolfi C, Ottolenghi S, Torella D, Nadal-Ginard B. Adult c-kitpos cardiac stem cells are necessary and sufficient for functional cardiac regeneration and repair. *Cell* 154: 827–842, 2013.
 23. Fisher SA, Doree C, Mathur A, Martin-Rendon E. Meta-analysis of cell therapy trials for patients with heart failure. *Circ Res* 116: 1361–1377, 2015.
 24. Frati C, Savi M, Graiani G, Lagrasta C, Cavalli S, Prezioso L, Rossetti P, Mangiaracina C, Ferraro F, Madeddu D, Musso E, Stilli D, Rossini A, Falco A, De Angelis A, Rossi F, Urbanek K, Leri A, Kajstura J, Anversa P, Quaini E, Quaini F. Resident cardiac stem cells. *Curr Pharm Des* 17: 2074–2099, 2011.
 25. Giuliani A, Frati C, Rossini A, Komlev VS, Lagrasta C, Savi M, Cavalli S, Gaetano C, Quaini F, Manescu A, Rustichelli F. High-resolution X-ray microtomography for three-dimensional imaging of cardiac progenitor cell homing in infarcted rat hearts. *J Tissue Eng Regen Med* 5: e168–e178, 2011.
 26. Gneccchi M, Zhang Z, Ni A, Dzau VJ. Paracrine mechanisms in adult stem cell signaling and therapy. *Circ Res* 103: 1204–1219, 2008.
 27. Hwang HJ, Chang W, Song BW, Song H, Cha MJ, Kim IK, Lim S, Choi EJ, Ham O, Lee SY, Shim J, Joung B, Pak HN, Kim SS, Choi BR, Jang Y, Lee MH, Hwang KC. Antiarrhythmic potential of mesenchymal stem cell is modulated by hypoxic environment. *J Am Coll Cardiol* 60: 1698–1706, 2012.
 28. Ihl-Vahl R, Eschenhagen T, Kübler W, Marquetant R, Nose M, Schmitz W, Scholz H, Strasser RH. Differential regulation of mRNA specific for beta 1- and beta 2-adrenergic receptors in human failing hearts. Evaluation of the absolute cardiac mRNA levels by two independent methods. *J Mol Cell Cardiol* 28: 1–10, 1996.
 29. Janse MJ, Opthof T, Kléber AG. Animal models of cardiac arrhythmias. *Cardiovasc Res* 39: 165–177, 1998.
 30. Kjekshus J. Arrhythmias and mortality in congestive heart failure. *Am J Cardiol* 65: 421–481, 1990.
 31. Kléber AG, Rudy Y. Basic mechanisms of cardiac impulse propagation and associated arrhythmias. *Physiol Rev* 84: 431–488, 2004.
 32. Kleber AG, Saffitz JE. Role of the intercalated disc in cardiac propagation and arrhythmogenesis. *Front Physiol* 5: 404, 2014.
 33. Koudstaal S, Bastings MM, Feyen DA, Waring CD, van Slochteren FJ, Danks PY, Torella D, Sluijter JP, Nadal-Ginard B, Doevendans PA, Ellison GM, Chamuleau SA. Sustained delivery of insulin-like growth factor-1/hepatocyte growth factor stimulates endogenous cardiac repair in the chronic infarcted pig heart. *J Cardiovasc Transl Res* 7: 232–241, 2014.
 34. Lai PF, Panama BK, Massé S, Li G, Zhang Y, Kusha M, Farid TA, Asta J, Backx PH, Yau TM, Nanthakumar K. Mesenchymal stem cell transplantation mitigates electrophysiological remodeling in a rat model of myocardial infarction. *J Cardiovasc Electrophysiol* 24: 813–821, 2013.
 35. Lammers WJ, Schalij MJ, Kirchhof CJ, Allesie MA. Quantification of spatial inhomogeneity in conduction and initiation of reentrant atrial arrhythmias. *Am J Physiol Heart Circ Physiol* 259: H1254–H1263, 1990.
 36. Lee PL, Pogwizd SM. Micropatterns of propagation. In: *Cardiovascular Gap Junctions. Advances in Cardiology*, vol. 42, edited by Dhein S. Basel, Switzerland: Karger, 2006.
 37. Leri A, Kajstura J, Anversa P. Role of cardiac stem cells in cardiac pathophysiology: a paradigm shift in human myocardial biology. *Circ Res* 109: 941–961, 2011.
 38. Li TS, Cheng K, Malliaras K, Smith RR, Zhang Y, Sun B, Matsushita N, Blusztajn A, Terrovitis J, Kusuoka H, Marbán L, Marbán E. Direct comparison of different stem cell types and subpopulations reveals superior paracrine potency and myocardial repair efficacy with cardiosphere-derived cells. *J Am Coll Cardiol* 59: 942–953, 2012.
 39. Linke A, Müller P, Nurzynska D, Casarsa C, Torella D, Nascimbene A, Castaldo C, Cascapera S, Böhm M, Quaini F, Urbanek K, Leri A, Hintze TH, Kajstura J, Anversa P. Stem cells in the dog heart are self-renewing, clonogenic, and multipotent and regenerate infarcted myocardium, improving cardiac function. *Proc Natl Acad Sci USA* 102: 8966–8971, 2005.
 40. Macchi E, Cavalieri M, Stilli D, Musso E, Baruffi S, Olivetti G, Ershler PR, Lux RL, Taccardi B. High-density epicardial mapping during current injection and ventricular activation in rat hearts. *Am J Physiol Heart Circ Physiol* 275: H1886–H1897, 1998.
 41. Makita N, Seki A, Sumitomo N, Chkourko H, Fukuhara S, Watanabe H, Shimizu W, Bezzina CR, Hasdemir C, Mugishima H, Makiyama T, Baruteau A, Baron E, Horie M, Hagiwara N, Wilde AA, Probst V, Le Marec H, Roden DM, Mochizuki N, Schott JJ, Delmar M. A Connexin40 mutation associated with a malignant variant of progressive familial heart block type I. *Circ Arrhythmia Electrophysiol* 5: 163–172, 2012.
 42. Makkar RR, Smith RR, Cheng K, Malliaras K, Thomson LE, Berman D, Czer LS, Marbán L, Mendizabal A, Johnston PV, Russell SD, Schuleri KH, Lardo AC, Gerstenblith G, Marbán E. Intracoronary

- cardiosphere-derived cells for heart regeneration after myocardial infarction (CADUCEUS): a prospective, randomised phase 1 trial. *Lancet* 379: 895–904, 2012.
43. Martinez M, Calvo Torrent A, Pico Alfonso MA. Social defeat and subordination as models of social stress in laboratory rodents: a review. *Aggress Behav* 24: 241–256, 1998.
 44. Menasché P. Cardiac cell therapy: lessons from clinical trials. *J Mol Cell Cardiol* 50: 258–265, 2011.
 45. Menasché P, Vanneaux V, Fabreguettes JR, Bel A, Tosca L, Garcia S, Bellamy V, Farouz Y, Pouly J, Damour O, Périer MC, Desnos M, Hagège A, Agbulut O, Bruneval P, Tachdjian G, Trouvin JH, Larghero J. Towards a clinical use of human embryonic stem cell-derived cardiac progenitors: a translational experience. *Eur Heart J* 36: 743–750, 2015.
 46. Mills WR, Mal N, Kiedrowski MJ, Unger R, Forudi F, Popovic ZB, Penn MS, Laurita KR. Stem cell therapy enhances electrical viability in myocardial infarction. *J Mol Cell Cardiol* 42: 304–314, 2007.
 47. Moller JE, Egstrup K, Kober L, Poulsen SH, Nyvad O, Torp-Pedersen C. Prognostic importance of systolic and diastolic function after acute myocardial infarction. *Am Heart J* 145: 147–153, 2003.
 48. Mount S, Davis DR. Electrical effects of stem cell transplantation for ischaemic cardiomyopathy: Friend or Foe? *J Physiol* 594: 2511–2524, 2016.
 49. Mozaffarian D, Benjamin EJ, Go AS, Arnett DK, Blaha MJ, Cushman M, de Ferranti S, Després JP, Fullerton HJ, Howard VJ, Huffman MD, Judd SE, Kissela BM, Lackland DT, Lichtman JH, Lisabeth LD, Liu S, Mackey RH, Matchar DB, McGuire DK, Mohler ER 3rd, Moy CS, Muntner P, Mussolino ME, Nasir K, Neumar RW, Nichol G, Palaniappan L, Pandey DK, Reeves MJ, Rodriguez CJ, Sorlie PD, Stein J, Towfighi A, Turan TN, Virani SS, Willey JZ, Woo D, Yeh RW, Turner MB; American Heart Association Statistics Committee and Stroke Statistics Subcommittee. Heart disease and stroke statistics-2015 update: a report from the American Heart Association. *Circulation* 131: e29–e322, 2015. (Corrigendum. *Circulation* 131: e98, 2015; *Circulation* 131: e117, 2015; *Circulation* 131: e163, 2015; *Circulation* 131: e319, 2015).
 50. Mureli S, Gans CP, Bare DJ, Geenen DL, Kumar NM, Banach K. Mesenchymal stem cells improve cardiac conduction by upregulation of Connexin43 through paracrine signaling. *Am J Physiol Heart Circ Physiol* 304: H600–H609, 2013.
 51. Nadal-Ginard B, Ellison GM, Torella D. The cardiac stem cell compartment is indispensable for myocardial cell homeostasis, repair and regeneration in the adult. *Stem Cell Res* 13: 615–630, 2014.
 52. Ogawa S, Furuno I, Satoh Y, Yoh S, Saeki K, Sadanaga T, Katoh H, Nakamura Y. Quantitative indices of dispersion of refractoriness for identification of propensity to re-entrant ventricular tachycardia in a canine model of myocardial infarction. *Cardiovasc Res* 25: 378–383, 1991.
 53. Okabe M, Ikawa M, Kominami K, Nakanishi T, Nishimune Y. ‘Green mice’ as a source of ubiquitous green cells. *FEBS Lett* 407: 313–319, 1997.
 54. Opthof T, Coronel R, Vermeulen JT, Verberne HJ, van Capelle FJ, Janse MJ. Dispersion of refractoriness in normal and ischaemic canine ventricle: effects of sympathetic stimulation. *Cardiovasc Res* 27: 1954–1960, 1993.
 55. Overholt ED, Joyner RW, Veenstra RD, Rawling D, Wiedmann R. Unidirectional block between Purkinje and ventricular layers of papillary muscles. *Am J Physiol Heart Circ Physiol* 247: H584–H595, 1984.
 56. Pak HN, Qayyum M, Kim DT, Hamabe A, Miyauchi Y, Lill MC, Frantzen M, Takizawa K, Chen LS, Fishbein MC, Sharifi BG, Chen PS, Makkar R. Mesenchymal stem cell injection induces cardiac nerve sprouting and increased tenascin expression in a Swine model of myocardial infarction. *J Cardiovasc Electrophysiol* 14: 841–848, 2003.
 57. Peters NS, Wit AL. Myocardial architecture and ventricular arrhythmogenesis. *Circulation* 97: 1746–1754, 1998.
 58. Piegari E, De Angelis A, Cappetta D, Russo R, Esposito G, Costantino S, Graiani G, Frati C, Prezioso L, Berrino L, Urbanek K, Quaini F, Rossi F. Doxorubicin induces senescence and impairs function of human cardiac progenitor cells. *Basic Res Cardiol* 108: 334, 2013.
 59. Roger VL. Epidemiology of heart failure. *Circ Res* 113: 646–659, 2013.
 60. Roell W, Lewalter T, Sasse P, Tallini YN, Choi BR, Breitbach M, Doran R, Becher UM, Hwang SM, Bostani T, von Maltzahn J, Hofmann A, Reining S, Eiberger B, Gabris B, Pfeifer A, Welz A, Willecke K, Salama G, Schrickel JW, Kotlikoff MI, Fleischmann BK. Engraftment of Connexin43-expressing cells prevents post-infarct arrhythmia. *Nature* 450: 819–824, 2007.
 61. Rohr S, Kucera JP. Involvement of the calcium inward current in cardiac impulse propagation: induction of unidirectional conduction block by nifedipine and reversal by Bay K 8644. *Biophys J* 72: 754–766, 1997.
 62. Rohr S, Kucera JP, Fast VG, Kléber AG. Paradoxical improvement of impulse conduction in cardiac tissue by partial cellular uncoupling. *Science* 275: 841–844, 1997.
 63. Rossini A, Frati C, Lagrasta C, Graiani G, Scopece A, Cavalli S, Musso E, Baccarin M, Di Segni M, Fagnoni F, Germani A, Quaini E, Mayr M, Xu Q, Barbuti A, DiFrancesco D, Pompilio G, Quaini F, Gaetano C, Capogrossi MC. Human cardiac and bone marrow stromal cells exhibit distinctive properties related to their origin. *Cardiovasc Res* 89: 650–660, 2011.
 64. Salameh A, Dhein S. Adrenergic control of cardiac gap junction function and expression. *Naunyn Schmiedeberg Arch Pharmacol* 383: 331–346, 2011.
 65. Rota M, Padin-Iruegas ME, Misao Y, De Angelis A, Maestroni S, Ferreira-Martins J, Fiumana E, Rastaldo R, Arcarese ML, Mitchell TS, Boni A, Bolli R, Urbanek K, Hosoda T, Anversa P, Leri A, Kajstura J. Local activation or implantation of cardiac progenitor cells rescues scarred infarcted myocardium improving cardiac function. *Circ Res* 103: 107–116, 2008.
 66. Salemi VM, Pires MD, Cestari IN, Cestari IA, Picard MH, Leirner AA, Mady C. Echocardiographic assessment of global ventricular function using the myocardial performance index in rats with hypertrophy. *Artif Organs* 28: 332–337, 2004.
 67. Sanganalath SK, Bolli R. Cell therapy for heart failure: a comprehensive overview of experimental and clinical studies, current challenges, and future directions. *Circ Res* 113: 810–834, 2013.
 68. Severs NJ, Dupont E, Thomas N, Kaba R, Rothery S, Jain R, Sharpey K, Fry CH. Alterations in cardiac connexin expression in cardiomyopathies. *Adv Cardiol* 42: 228–242, 2006.
 69. Severs NJ, Bruce AF, Dupont E, Rothery S. Remodelling of gap junctions and connexin expression in diseased myocardium. *Cardiovasc Res* 80: 9–19, 2008.
 70. Sgoifo A, Koolhaas J, De Boer S, Musso E, Stilli D, Buwalda B, Meerlo P. Social stress, autonomic neural activation, and cardiac activity in rats. *Neurosci Biobehav Rev* 23: 915–923, 1999.
 71. Sgoifo A, Stilli D, Medici D, Gallo P, Aimi B, Musso E. Electrode positioning for reliable telemetry ECG recordings during social stress in unrestrained rats. *Physiol Behav* 60: 1397–1401, 1996.
 72. Shiba Y, Fernandes S, Zhu WZ, Filice D, Muskheli V, Kim J, Palpant NJ, Gantz J, Moyes KW, Reinecke H, Van Biber B, Dardas T, Mignone JL, Izawa A, Hanna R, Viswanathan M, Gold JD, Kotlikoff MI, Sarvazyan N, Kay MW, Murry CE, Laflamme MA. Human ES-cell-derived cardiomyocytes electrically couple and suppress arrhythmias in injured hearts. *Nature* 489: 322–325, 2012.
 73. Smit NW, Coronel R. Stem cells can form gap junctions with cardiac myocytes and exert pro-arrhythmic effects. *Front Physiol* 5: 419, 2014.
 74. Smith RR, Barile L, Messina E, Marbán. Stem cells in the heart: what’s the buzz all about? Part 2: Arrhythmic risks and clinical studies. *Heart Rhythm* 5: 880–887, 2008.
 75. Spach MS, Heidlage JF, Dolber PC, Barr RC. Electrophysiological effects of remodeling cardiac gap junctions and cell size: Experimental and model studies of normal cardiac growth. *Circ Res* 86: 302–311, 2000.
 76. Stein PK, Bosner MS, Kleiger RE, Conger BM. Heart rate variability: a measure of cardiac autonomic tone. *Am Heart J* 127: 1376–1381, 1994.
 77. Stilli D, Bocchi L, Berni R, Zaniboni M, Cacciani F, Chaponnier C, Musso E, Gabbiani G, Clément S. Correlation of alpha-skeletal actin expression, ventricular fibrosis and heart function with the degree of pressure overload cardiac hypertrophy in rats. *Exp Physiol* 91: 571–580, 2006.
 78. Strauer BE, Steinhoff G. 10 years of intracoronary and intramyocardial bone marrow stem cell therapy of the heart: from the methodological origin to clinical practice. *J Am Coll Cardiol* 58: 1095–1104, 2011.
 79. Taccardi B, Punske BB, Macchi E, Macleod RS, Ershler PR. Epicardial and intramural excitation during ventricular pacing: effect of myocardial structure. *Am J Physiol Heart Circ Physiol* 294: H1753–H1766, 2008.
 80. Tang XL, Rokosh G, Sanganalath SK, Yuan F, Sato H, Mu J, Dai S, Li C, Chen N, Peng Y, Dawn B, Hunt G, Leri A, Kajstura J, Tiwari S, Shirk G, Anversa P, Bolli R. Intracoronary administration of cardiac

- progenitor cells alleviates left ventricular dysfunction in rats with a 30-day-old infarction. *Circulation* 121: 293–305, 2010.
81. Tillmanns J, Rota M, Hosoda T, Misao Y, Esposito G, Gonzalez A, Vitale S, Parolin C, Yasuzawa-Amano S, Muraski J, De Angelis A, Lecapitaine N, Siggins RW, Loredi M, Bearzi C, Bolli R, Urbanek K, Leri A, Kajstura J, Anversa P. Formation of large coronary arteries by cardiac progenitor cells. *Proc Natl Acad Sci USA* 105: 1668–1673, 2008.
 82. Urbanek K, Rota M, Cascapera S, Bearzi C, Nascimbene A, De Angelis A, Hosoda T, Chimenti S, Baker M, Limana F, Nurzynska D, Torella D, Rotatori F, Rastaldo R, Musso E, Quaini F, Leri A, Kajstura J, Anversa P. Cardiac stem cells possess growth factor-receptor systems that after activation regenerate the infarcted myocardium, improving ventricular function and long-term survival. *Circ Res* 97: 663–673, 2005. (Corrigendum. *Circ Res* 98: e27, 2006).
 83. Ursell PC, Gardner PI, Albala A, Fenoglio JJ Jr, Wit AL. Structural and electrophysiological changes in the epicardial border zone of canine myocardial infarcts during infarct healing. *Circ Res* 56: 436–451, 1985.
 84. van Berlo JH, Kanisicak O, Maillet M, Vagnozzi RJ, Karch J, Lin SC, Middleton RC, Marbán E, Molkentin JD. c-kit⁺ cells minimally contribute cardiomyocytes to the heart. *Nature* 509: 337–341, 2014.
 85. van der Heyden MA, Wijnhoven TJ, Opthof T. Molecular aspects of adrenergic modulation of the transient outward current. *Cardiovasc Res* 71: 430–442, 2006.
 86. van Rijen HV, Eckardt D, Degen J, Theis M, Ott T, Willecke K, Jongsma HJ, Opthof T, de Bakker JM. Slow conduction and enhanced anisotropy increase the propensity for ventricular tachyarrhythmias in adult mice with induced deletion of Connexin43. *Circulation* 109: 1048–1055, 2004.
 87. van Rijen HV, van Veen TA, Gros D, Wilders R, de Bakker JM. Connexins and cardiac arrhythmias. *Adv Cardiol* 42: 150–160, 2006.
 88. Walker MJ, Curtis MJ, Hearse DJ, Campbell RWF, Janse MJ, Yellon DM, Cobbe SM, Coker SJ, Harness JB, Harron DWG, Higgins AJ, Julian DG, Lab MJ, Manning AS, Northover BJ, Parratt JR, Riemersma RA, Riva E, Russell DC, Sheridan DJ, Winslow E, Woodward B. The Lambeth Conventions: guidelines for the study of arrhythmias in ischaemia, infarction, and reperfusion. *Cardiovasc Res* 22: 447–455, 1988.
 89. Wang D, Zhang F, Shen W, Chen M, Yang B, Zhang Y, Cao K. Mesenchymal stem cell injection ameliorates the inducibility of ventricular arrhythmias after myocardial infarction in rats. *Int J Cardiol* 152: 314–320, 2011.
 90. Wang Y, Xue M, Xuan YL, Hu HS, Cheng WJ, Suo F, Li XR, Yan SH, Wang LX. Mesenchymal stem cell therapy improves diabetic cardiac autonomic neuropathy and decreases the inducibility of ventricular arrhythmias. *Heart Lung Circ* 22: 1018–1025, 2013.
 91. Wit AL, Peters NS. The role of gap junctions in the arrhythmias of ischemia and infarction. *Heart Rhythm* 9: 308–311, 2012.
 92. Zhang F, Song G, Li X, Gu W, Shen Y, Chen M, Yang B, Qian L, Cao K. Transplantation of iPSC ameliorates neural remodeling and reduces ventricular arrhythmias in a post-infarcted swine model. *J Cell Biochem* 115: 531–539, 2014.
 93. Zheng SX, Weng YL, Zhou CQ, Wen ZZ, Huang H, Wu W, Wang JF, Wang T. Comparison of cardiac stem cells and mesenchymal stem cells transplantation on the cardiac electrophysiology in rats with myocardial infarction. *Stem Cell Rev* 9: 339–349, 2013.

